JOURNAL OF GEOPHYSICAL RESEARCH, VOL. 112, C02005, doi:10.1029/2005JC003416, 2007

Atlantic water circulation over the Mendeleev Ridge and Chukchi Borderland from thermohaline intrusions and water mass properties

Rebecca A. Woodgate,[1] Knut Aagaard,[1] James H. Swift,[2] William M. Smethie Jr.,[3] and Kelly K. Falkner[4]

Received 23 November 2005; revised 8 August 2006; accepted 19 September 2006; published 3 February 2007.

[1] Hydrographic and tracer data from 2002 illustrate Atlantic water pathways and variability in the Mendeleev Ridge and Chukchi Borderland (CBLMR) region of the Arctic Ocean. Thermohaline double diffusive intrusions (zigzags) dominate both the Fram Strait (FSBW) and Barents Sea Branch Waters (BSBW) in the region. We show that details of the zigzags' temperature-salinity structure partially describe the water masses forming the intrusions. Furthermore, as confirmed by chemical tracers, the zigzags' peaks contain the least altered water, allowing assessment of the temporal history of the Atlantic waters. Whilst the FSBW shows the 1990s warming and then a slight cooling, the BSBW has continuously cooled and freshened over a similar time period. The newest boundary current waters are found west of the Mendeleev Ridge in 2002. Additionally, we show the zigzag structures can fingerprint various water masses, including the boundary current. Using this, tracer data and the advection of the 1990s warming, we conclude the strongly topographically steered boundary current, order 50 km wide and found between the 1500 m and 2500 m isobaths, crosses the Mendeleev Ridge north of 80°N, loops south around the Chukchi Abyssal Plain and north around the Chukchi Rise, with the 1990s warming having reached the northern (but not the southern) Northwind Ridge by 2002. Pacific waters influence the Atlantic layers near the shelf and over the Chukchi Rise. The Northwind Abyssal Plain is comparatively stagnant, being ventilated only slowly from the north. There is no evidence of significant boundary current flow through the Chukchi Gap.

Citation: Woodgate, R. A., K. Aagaard, J. H. Swift, W. M. Smethie Jr., and K. K. Falkner (2007), Atlantic water circulation over the Mendeleev Ridge and Chukchi Borderland from thermohaline intrusions and water mass properties, *J. Geophys. Res.*, *112*, C02005, doi:10.1029/2005JC003416.

1. Introduction

[2] Recent reports of continuing change in the northern high latitudes [e.g., *Morison et al.*, 2000; *Polyakov et al.*, 2005] make it increasingly important to understand the Arctic Ocean and its circulation. Surprisingly little is known about ocean pathways and flow structures, especially of the subsurface waters. Yet, this basic information is essential for understanding Arctic climate and climate change; for studying chemical and geochemical cycling; and for validating and improving the growing array of conceptual models and high-resolution computer simulations of the Arctic, several of which yield significantly differing versions of Arctic Ocean circulation [e.g., *Proshutinsky et al.*, 2005].

[3] Although satellites and drifting buoys allow large scale, semi-continuous measurement of the surface flow and ice conditions, below a few tens of meters the subsurface flow in much of the Arctic Ocean appears to be mostly decoupled from the surface circulation [*Aagaard*, 1989; *Jones et al.*, 1998]. Apart from upper-ocean boundary layer work [e.g., *Hunkins*, 1966; *McPhee and Smith*, 1976] and observations taken from buoys moored to the drifting ice [e.g., *Plueddemann et al.*, 1998; *Shimada et al.*, 2004], direct velocity measurements in the Arctic Ocean are very sparse, especially measurements of significant temporal extent or away from the shelves. The subsurface circulation has thus generally been inferred from a combination of hydrographic and tracer measurements. These data, combined with the sparse direct current measurements, suggest a low kinetic energy ocean with weak interior flow, populated by eddies, and with a stronger (though still relatively weak) cyclonic boundary current along the margins of the ocean basins [e.g., *Aagaard*, 1989; *Rudels et al.*, 1994; *Jones*, 2001].

[4] This boundary current is the major organized subsurface transport mechanism for mass, heat, tracers, and contaminants in the Arctic Ocean [*Aagaard*, 1989; *Carmack et al.*, 1997; *Smith et al.*, 1998, 1999]. It carries the Atlantic-

[1]Polar Science Center, Applied Physics Laboratory, University of Washington, Seattle, Washington, USA.
[2]Scripps Institution of Oceanography, University of California, San Diego, California, USA.
[3]Lamont-Doherty Earth Observatory of Columbia University, Palisades, New York, USA.
[4]College of Oceanic and Atmospheric Sciences, Oregon State University, Corvallis, Oregon, USA.

0148-0227/07/2005JC003416$09.00

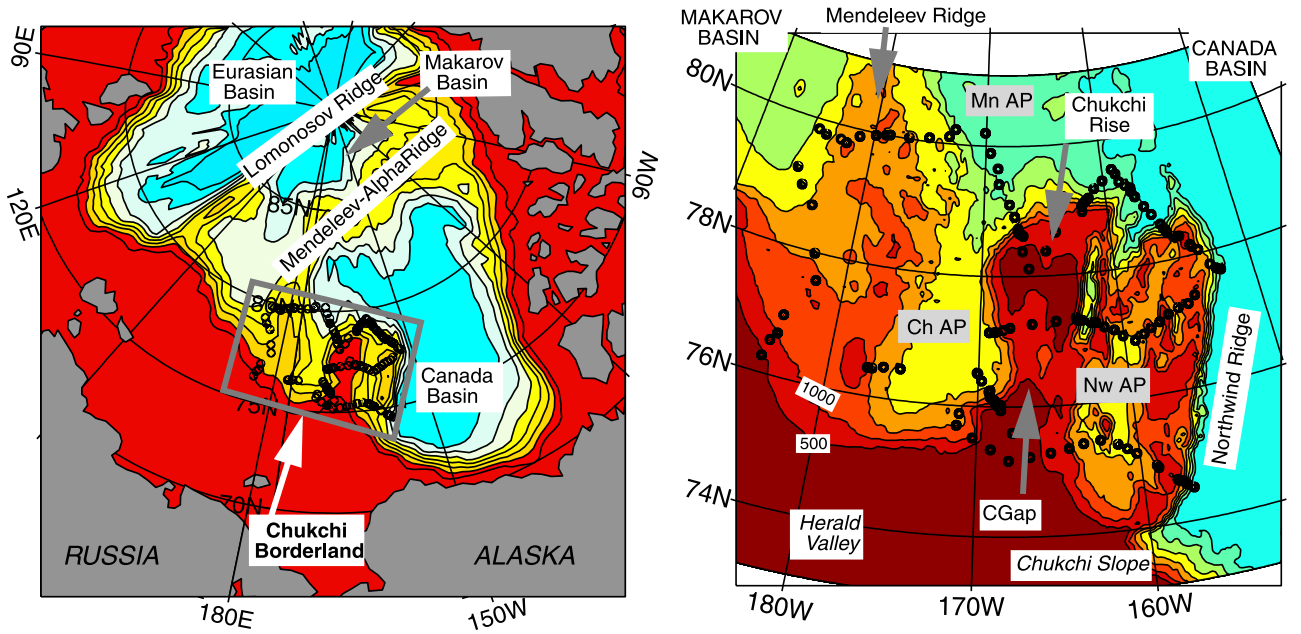

Figure 1. Maps of the study region. (left) Position of the Chukchi Borderland and Mendeleev Ridge in relation to the rest of the Arctic. (right) Focus on the region marked by a grey box in the left panel, and shows details of the bathymetry in the Mendeleev Ridge and Chukchi Borderland (CBLMR) area. Black dots mark the CTD casts of the CBL2002 research cruise on the USCGC Polar Star. Depth contours are (left) schematic and (right) from IBCAO, at depth interval of 500 m. Major geographical features are labeled, with abbreviations for Mendeleev Abyssal Plain (Mn AP); Chukchi Abyssal Plain (Ch AP), Northwind Abyssal Plain (Nw AP), and Chukchi Gap (CGap). Herald Valley and the Chukchi Slope extend off the bottom of the map.

origin waters that enter the Arctic through the Fram Strait (the warm, salty core at ~300 m in the Arctic, referred to as the Fram Strait Branch Water, FSBW) and the Barents Sea (cooler water at ~700 m in the Arctic, referred to as the Barents Sea Branch Water, BSBW) around the southern boundary of the Eurasian Basin to the junction of the Lomonosov Ridge and the Eurasian continent [*Schauer et al.*, 1997]. Year-long moored current measurements from 1995–1996 [*Woodgate et al.*, 2001] show that the current, which is present over the 500–3000 m isobaths and equivalent barotropic [*Killworth*, 1992] in vertical structure (therefore topography-following), is split at this point by the topography, with (in this year) about half turning northward towards Greenland along the Eurasian flank of the Lomonosov Ridge, while the other half continues into the Canadian Basin. Hydrographic data from the same time period suggest that some of the flow diverted northward actually crosses over the ridge south of 88°N and returns southward along the Canadian flank, possibly rejoining the eastward flowing boundary current over the continental slope [*Woodgate et al.*, 2001; *Schauer et al.*, 2002].

[5] East of the Eurasian end of the Lomonosov Ridge, the cyclonic pathway of the boundary current is less well documented. The eastward flow next encounters the broad Mendeleev Ridge and the large region of complex topography north of the Chukchi Sea, known as the Chukchi Borderland, both of which it must traverse to reach the Canada Basin by a continental slope route (Figure 1).

[6] The Mendeleev Ridge, although topographically less distinct than the Lomonosov Ridge, is generally believed to mark the boundary between the Atlantic- and Pacific-dominated domains (or "water mass assemblies") in the Arctic Ocean at this time [*Carmack et al.*, 1995; *McLaughlin et al.*, 1996; *Morison et al.*, 1998; *Swift et al.*, 2005]. This is particularly clear in the halocline waters, and there have certainly been indications that a portion of the boundary current is diverted into the interior Arctic Ocean along the Mendeleev Ridge [*Swift et al.*, 1997].

[7] The Chukchi Borderland is a much more tortuous topographic feature. It consists of the shallow (rising to less than 200 m in places), ca. 200 km long Chukchi Rise in the west; and the Northwind Ridge in the east (shallowest depths order 1000 m); separated by the Northwind Abyssal Plain (deepest regions around 3000 m). (The Chukchi Rise is also known in the literature as the Chukchi Cap. We use Chukchi Rise in this paper to avoid confusion with the Chukchi Gap, the ca. 1000 m deep channel separating the Chukchi Rise from the Chukchi slope.) Tracer measurements from the central Arctic Ocean [*Smith et al.*, 1999; *Smethie et al.*, 2000] suggest that a portion of the boundary current is also separated from the continental margin by the complex Chukchi Borderland. A modified Atlantic layer does reach the Canada Basin, as is evident from the temperature maximum found there [*Swift et al.*, 1997], although the vertical water mass structure is rather different from that in the Eurasian Basin [*McLaughlin et al.*, 1996].

[8] In the early 1990s anomalously warm Atlantic water entered the Arctic Ocean via the Fram Strait [*Quadfasel et al.*, 1991, 1993]. Tracing this warm anomaly around the Arctic basins has confirmed some of these transport pathways and suggested transit times [*Swift et al.*, 1997; *Karcher et al.*, 2003; *Polyakov et al.*, 2005], although these

conclusions generally yield transit estimates significantly faster than those calculated from tracer mixing data [e.g., *Frank et al.*, 1998]. Recent work by *Shimada et al.* [2004] traces this temperature anomaly through the Chukchi Borderland region between 1993 and 2003, suggesting two pathways for the Fram Strait Branch Water - one via the ''Chukchi Gap'' to the Beaufort Slope, and the other spreading eastward from the northern tip of the Northwind Ridge (Figure 1). We will return to the spreading of this temperature anomaly in sections 3 and 5.

[9] Note that the driving mechanism for the boundary current is far from fully understood. The failure of main state-of-the-art models to agree on a simulated Atlantic water circulation (including the direction of flow in some regions, especially in the western Arctic [*Proshutinsky et al.*, 2005]) may be due to resolution issues, or subgrid-scale parameterizations. *Nazarenko et al.* [1997] introduce the ''Neptune'' effect, a subgrid-scale forcing based on eddy-topography interactions, to obtain a realistic circulation. More recently, an idealized study by *Yang* [2006] suggests that the balance of potential vorticity inputs from the Bering and Fram Straits may determine the cyclonic/anticyclonic nature of the large-scale Atlantic water circulation. In all cases, it is clear that further observations of the properties of the boundary current are necessary as an input for both theoretical and modeling studies.

[10] In the current paper, we draw on high resolution hydrographic and tracer data from a late summer cruise to the Chukchi Borderland and Mendeleev Ridge (CBLMR) region in 2002, to investigate these water pathways over a larger geographical area and in more detail than the previous, *Shimada et al.* [2004] work, which considered only the Fram Strait Branch Water. Our data indicate that near the boundaries, the Arctic Ocean contains dramatic, sharp frontal features suggestive of well-confined currents. Full depth casts and chemical tracer data allow us also to study the structures of both the Fram Strait Branch Water and the deeper, Barents Sea Branch Water and determine primary pathways and quasi-stagnation zones. Particular use will be made of the remarkable interleaving structures in temperature and salinity, so ubiquitous in the 1980s and 1990s in the Eurasian Basin, and later (1993 and 1994) found also in the Makarov Basin [*Carmack et al.*, 1998], although not until recently observed in the Canada Basin [*Melling*, 1998; *McLaughlin et al.*, 2002, 2004]. Section 2 summarizes the data set used in this study. Section 3 considers the historic translation of the 1990s Atlantic temperature anomaly through the Mendeleev Ridge and Chukchi Borderland region. Section 4 addresses the characteristic interleaving of temperature and salinity in both the Fram Strait and Barents Sea branches of the Atlantic layer, discussing the various forms and tracer signals, to make inferences on formation mechanisms and geographical variability. Finally, section 5 combines these inferences to suggest pathways and transit times for the Atlantic water circulation.

2. Data Overview

[11] In August/September 2002, a high resolution hydrographic data set from the Mendeleev Ridge and Chukchi Borderland region was collected during a 5 week cruise (CBL2002) of the USCGC Polar Star. The 126 stations (Figure 1) were aligned in a series of sections, designed to cross the boundary current at a number of locations, in particular to section it upstream and downstream of regions where it has been suggested that separation of the boundary current occurs or that waters are otherwise diverted into the interior. Reflecting the hypothesis of a topography-following current, station locations were (in part) determined by water depth, so that (within the usual constraints of operating in ice) station spacing was small ($\sim$5 km) over steep slopes and greater ($\sim$25 km) over the flatter regions.

[12] Full depth CTD-O (profiles of temperature, conductivity and dissolved oxygen) data, with bottle samples for salinity, dissolved oxygen, CFC and nutrients were collected to WOCE standards. Unless stated otherwise, all data cited in the paper are 2 db averages from the downcast. Data are accurate to $\sim$0.002°C; $\sim$0.002 psu; $\sim$1 dbar; $<$2 μmol/kg (CTD-oxygen, calibrated against bottle samples); $<$1 μmol/kg (silicate); and the larger of 0.01 pmol/kg or 1% (CFC-11). The full depth dissolved oxygen profiles were obtained using a single pumped SBE43 sensor. As the sensor is comparatively new [*Falkner et al.*, 2005], protocols are still being standardized. Temperature hysteresis and velocity profiling issues need to be addressed for the accurate processing of the data. For full details of the processing, see *Woodgate et al.* [2003]. The net result is a data set that is considered accurate to $<$2 μmol/kg, although the data are treated with caution in regions of extreme temperature gradients.

[13] Our analysis uses both CFC-11 and oxygen data to assess the ''age'' of a water mass, namely, the time since the water mass was last in contact with the atmosphere. A major strength of CFC-11 is that it is a conservative tracer, and changes in concentration reflect mixing with waters of differing CFC content. A disadvantage of the data is that values may only be measured by bottle samples, thus vertical profiles are discrete, not continuous. The new SBE43 oxygen sensor, in contrast, does gives a continuous vertical profile; however, dissolved oxygen is not a conservative tracer. Even in deep, isolated waters, oxygen values slowly decay due to biological activity. In productive areas (such as the Chukchi Sea), oxygen values can be substantially altered by biological processes. Thus, whilst low CFC-11 values indicate old waters, low oxygen values may reflect either old waters or new waters which have supported significant biological activity. In this paper we combine the various strengths of CFC-11 and oxygen data to infer ''age'' information for the full depth of the profiles.

3. Progression of the Fram Strait Branch Water Temperature Maximum Through the Mendeleev Ridge and Chukchi Borderland Region

[14] During the last decade, the temperature maximum of the Atlantic layer has been used as a tracer of Arctic Ocean circulation. *Quadfasel et al.* [1991, 1993] first reported that the Atlantic water temperature maximum north of Frans Joseph Land in 1990 was significantly warmer than climatology. Data from a cruise of the Canadian vessel Larsen in 1993 indicated the Atlantic waters at the southern end of the Mendeleev Ridge were warmer than historic data [*Carmack et al.*, 1995] and suggested a displacement of the front between the Atlantic and Pacific waters from the Lomono-

sov Ridge to the Mendeleev Ridge [*McLaughlin et al.*, 1996]. Data from the US submarine Pargo in 1993 also indicated the influence of the Atlantic water was increasing in the Arctic [*Morison et al.*, 1998]. The Arctic Ocean Section in 1994 [*Aagaard et al.*, 1996] confirmed these changes over the Lomonosov and Mendeleev Ridges [*Carmack et al.*, 1997; *Swift et al.*, 1997] and introduced the remarkable fact (we return to below) that thermohaline intrusions - inversions of temperature and salinity - in the depth range of the Atlantic water flows, were aligned in potential temperature (θ) - salinity (S) space throughout much of the Arctic. We note in passing that mooring and CTD data from the Eurasian end of the Lomonosov Ridge from 1995–1996 [*Woodgate et al.*, 2001] suggested a slight cooling ($\sim$0.5°C) of the Atlantic core following the warming, a conclusion supported by data from the central Lomonosov Ridge in 1995–1998 [*Gunn and Muench*, 2001]. Perhaps the most complete observational picture of changes in the temperature maximum in the Arctic in the 1980s and 1990s is given by *Karcher et al.* [2003], who compare all available observations with results from a high resolution computer model. Both observational and modeling studies suggest the warming is due to an increased inflow of anomalously warm Atlantic water [*Grotefendt et al.*, 1998; *Zhang et al.*, 1998; *Gerdes et al.*, 2003; *Karcher et al.*, 2003], which in turn is related to atmospheric circulation patterns [e.g., *Dickson et al.*, 2000]. In this context, it is interesting to note that studies of historic data suggest significant variability in Atlantic water temperatures. *Polyakov et al.* [2004], using data from 1893 to 2002, suggest a warm period in the 1930s and 1940s and in recent decades. *Swift et al.* [2005] (corrected ftp site: ftp://odf.ucsd.edu/pub/jswift/arctic_aari_method_B), drawing on a yearly version (from 1948 to 1993) of the publicly available decadal EWG data set, find the warming of the 1990s is not unique, and that the Atlantic layer was also warmer than the climatology in the 1950s and for the period of 1964–1969. Note also the *Swift et al.* [2005] study suggests that the movement of the Atlantic/Pacific front from the Lomonosov to the Mendeleev Ridge occurred in the mid 1980s, several years before the warming of the Atlantic layer.

[15] The available data suggest that the 1990s warming of the Atlantic layer is only evident over the Chukchi Borderland (CBL) region in the second half of the 1990s [*McLaughlin et al.*, 2004; *Shimada et al.*, 2004]. Using physical and geochemical data from the SHEBA drift of 1997–1998, *McLaughlin et al.* [2004] document the arrival of the warming and suggest two pathways through the CBL region, namely, one over the northern flank of the Chukchi Rise and one along the shelf break via the "Chukchi Gap" at ca. 76.5°N 168°W. *Shimada et al.* [2004] extend this analysis, looking at temperature on the 27.90 kg/m^3 sigma-0 surface combined in 3-year time intervals from 1990–2003, and suggest the warmer Atlantic water is absent from the CBL region up till 1995 and then spreads through the region until 2003.

[16] Figure 2 presents a similar analysis, although now broadened to the Mendeleev Ridge and CBL region and presented year-by-year for greater temporal resolution. For much of these data (mostly XCTD data from the SCICEX missions) the salinity records are noisy and of low accuracy. Thus we present the temperature maximum in the Atlantic layer rather than the temperature maximum on a specific density surface. Also, to illustrate pathways, we use yearly data rather than 3-year combinations. Note that, in a year, a signal advecting at 2 cm/s (the boundary current velocity estimated east of the Lomonosov Ridge by *Woodgate et al.* [2001]) would move $\sim$600 km, i.e., $\sim$6 degrees of latitude or $\sim$20 degrees of longitude at $\sim$75°N.

[17] In Figure 2, data from the eastern Mendeleev Ridge (ca. 80°N 178°W), from which several casts are available in 1994, 1997 and 2002, imply a warming through both these periods. The 1994 data also possibly suggest the warming signal moving south along the eastern side of the Mendeleev Ridge and then east along the south side of the Chukchi Abyssal Plain. Data from 2000 and 2002 confirm a warming in this region at ca. 75.5°N 172°W compared to 1994. Directly west of the Chukchi Rise, there appears to be a dramatic change between 1996 and 1997, although in general, temperatures on top of the Rise appear to be cooler than temperatures over the slope of the Rise, and thus care must be taken to compare similarly located stations. Over the Chukchi Rise itself, there is a clear change between 1993 and 2002, with the 1996 and 1997 data suggesting again a large part of the change occurs at that time. Northeast of the Chukchi Rise (ca. 79°N 158°W), only sections from 1998, 1999, 2000 and 2002 are similar enough in location to be comparable. They indicate a warming through these years. Similarly, just southeast of this (ca. 76.5°N 157°W), data suggest a warming compared to 1993 conditions.

[18] Thus, the most basic conclusions are still clear - since 1993 there has been a substantial warming throughout the Mendeleev Ridge and Chukchi Borderland region. In 1998–2000, there is a warmer region northeast of the Chukchi Rise. There is even some slight suggestion in Figure 2 of a modest cooling following the warming west of the Mendeleev Ridge. However, it is also clear that there is a significant amount of spatial variation over this area, even (as we will see below) on very short spatial scales, and that this, combined with differing station locations from year to year, significantly complicate the interpretation of these data as a time series. Some of this spatial variation is, as we will show below, due to sharp fronts in the Arctic Ocean. Some of this spatial variation is due to the thermohaline intrusions discussed above and below. The presence of thermohaline intrusions motivates the choice of the 27.90 kg/m^3 sigma-0 surface made by *Shimada et al.* [2004] since the intrusive steps are relatively small on this surface. An alternative approach (also used by *Shimada et al.* [2004]) is some form of vertical averaging.

[19] In this paper, we will take a third approach and use the structure of the thermohaline intrusions to further our understanding of the circulation pathways in this region of the Arctic. A mapping of thermohaline intrusions has been suggested in conference presentations by Carmack et al. (AGU 2004), McLaughlin et al. (AGU 2004) and Woodgate et al. (CliC Conference 2005). The first two presentations considered the progression of intrusions over time (from 1993 to 2004) from the Chukchi Borderland region into the Canada Basin. The third presentation considered instead the variety of intrusive forms found in the CBLMR region in one year (2002). In the present paper, we extend this latter

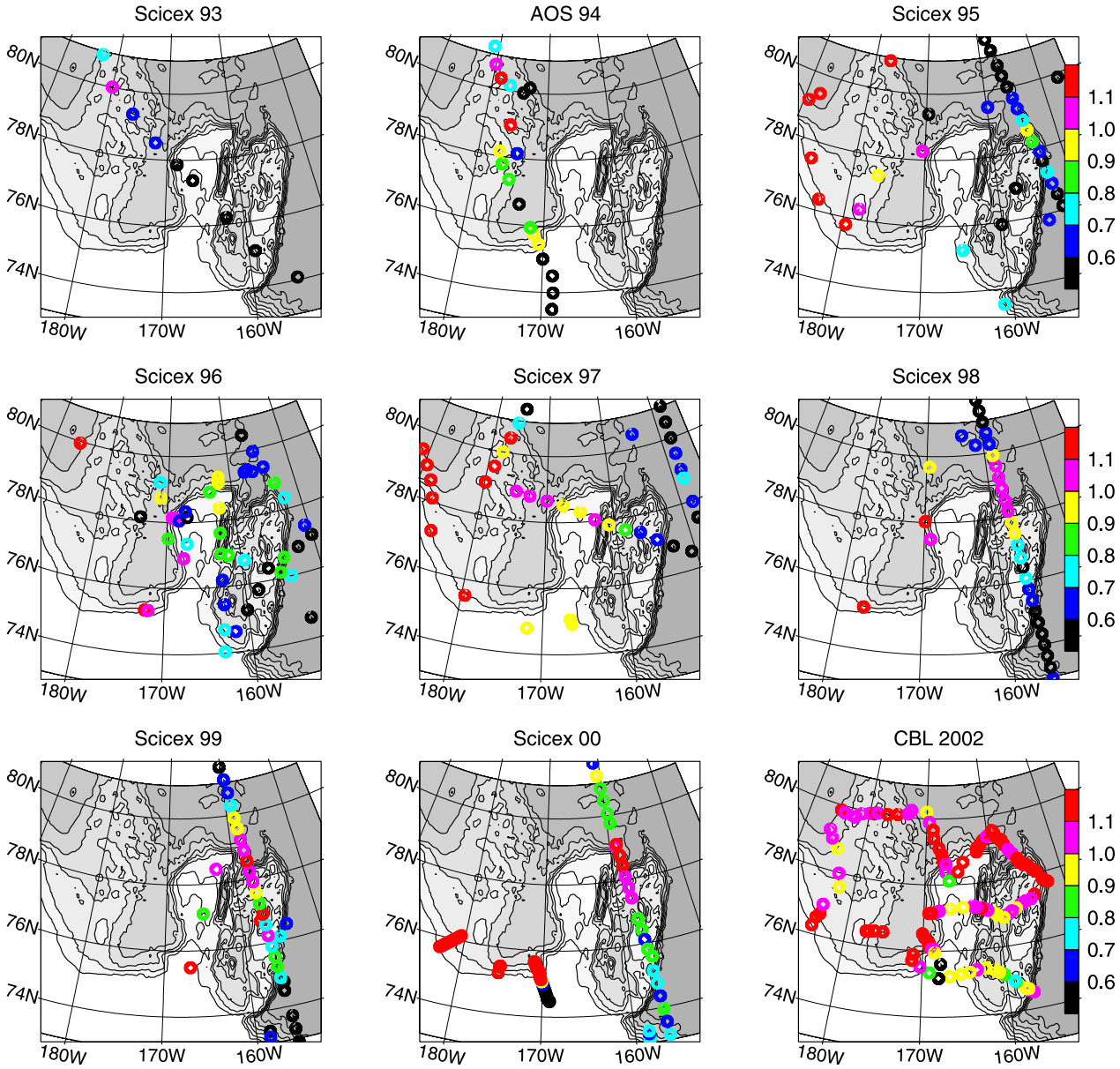

Figure 2. Plots of CTD, XBT or XCTD data from a variety of Arctic missions, taking place between 1993 (top left) and 2002 (bottom right). Dot color (as per color bar) indicates maximum temperature (in °C) deeper than 150 db, i.e., the temperature maximum in the Atlantic water layers. Depth contours are from IBCAO, at depth interval of 500 m. See section 3 for discussion.

analysis, in particular by using physical arguments to interpret details of the forms of the intrusions, in order to extract information on formation processes and parents water masses.

4. Thermohaline Intrusions in the Arctic's Atlantic Water Layers

[20] Whilst small amplitude (~0.02°C, ~0.01‰) temperature and salinity steps have been observed in the central Arctic since 1969 [*Neshyba et al.*, 1971; *Padman and Dillon*, 1987], the larger magnitude (~0.1°C) thermohaline intrusions of the Arctic Ocean were observed in 1981 during the EUBEX experiment north of Svalbard [*Perkin and Lewis*, 1984; *Rudels*, 1989] and were attributed to the interaction between the ambient Arctic waters and the warm Atlantic waters entering the Arctic via Fram Strait. In many locations away from Fram Strait, the appearance of the 1990s Atlantic water warming and the observation of intrusions do appear linked in time [see also *Carmack et al.*, 1998], although this may be a sampling artifact. Distinctive intrusions are present in the Rossiya 1990 data in the Eurasian Basin, especially off the north coast of the Barents Sea [*Quadfasel et al.*, 1993] and in the Oden 1991 data from the Eurasian Basin [*Anderson et al.*, 1994]. The Polarstern 1993 data [*Schauer et al.*, 1997] record the interleaving of Fram Strait and Barents Sea Branch waters off the northern slope of the Barents Sea; and the Larsen 1993 data, measuring the warming of the Atlantic layer at the Mendeleev Ridge, also exhibit distinctive thermohaline

intrusions [*Carmack et al.*, 1995]. Although north of Svalbard and near the Barents Sea (an hypothesized region of initiation of the intrusions) the θ-S structures are complex, away from these regions the "zigzag" structure of the intrusion is frequently very clean. The AOS 1994 trans-Arctic section shows the thermohaline intrusion structure throughout the Arctic, indicating (remarkably) that the zigzags are aligned ("nested") in θ-S space through the Arctic Ocean [*Carmack et al.*, 1997, 1998].

[21] The wealth of theoretical and experimental literature on these and similar thermohaline intrusive structures [e.g., *Turner*, 1965; *Stern*, 1967; *Ruddick and Turner*, 1979; *Toole and Georgi*, 1981; *McDougall*, 1985a, 1985b, 1986; *Walsh and Ruddick*, 1995, 1998, and references therein] shows the structures (especially the clean zigzag structures) to be due to double diffusive processes - a combination of salt fingering (instabilities growing from a water column stably stratified for temperature, but unstably stratified for salinity) and diffusive convection (instabilities growing from a water column stably stratified for salinity, but unstably stratified for temperature), due most fundamentally to the fact that heat diffuses faster than salt.

[22] Although there is still debate about the roles of salt-fingering versus diffusive convection in the formation of the intrusions within the Arctic [e.g., *May and Kelley*, 2001], analysis shows most generally that (amongst other results) these structures can be formed from suitably stratified horizontal fronts [e.g., *Ruddick and Turner*, 1979]; that intrusions spread across the front, with zero velocity in the along-front direction [*McDougall*, 1985a]; and that a finite amplitude, steady state is possible [*McDougall*, 1985b; *Walsh and Ruddick*, 1998]. Furthermore, specific theories have been put forward for the particular features of the Arctic intrusions. *Rudels et al.* [1999] collate observations from the Eurasian and Makarov Basin and speculate on formation mechanisms over narrow and wide fronts. *Walsh and Carmack* [2002] note that the intrusions appear not to travel into colder water, and show theoretically that the temperature dependence of the thermal expansion coefficient may explain this. *Walsh and Carmack* [2003] attribute the nested structure of the intrusions to slantwise convection, although the alignment of the intrusions in θ-S space throughout the Arctic is frequently considered to be due to advection without mixing, sometimes cited as the advection of "fossil" intrusions.

4.1. Lessons From Structures in θ-S Space

[23] There is a further property of the θ-S zigzag structure, which proves extremely useful, but has (to date) been neglected, namely the information contained in the zigzag structure about the parent water columns from which the zigzags are formed.

[24] Figure 3a shows the standard result that mechanical mixing in θ-S space can only create water masses that lie on a straight line between the two parent water masses. Consider now double diffusive processes - these allow temperature to equilibrate faster than salinity, with the resultant as shown schematically in the figure. Some combination of double diffusion and mechanical mixing may allow more of the θ-S space to be accessible (dark grey area of Figure 3a), but some fundamentals remain - i.e. without external sources, the θ-S resulting from the combination of two water parcels must have θ-S properties within the range of properties of the parents (light grey area of Figure 3a).

[25] Figure 3b shows schematically two parent water columns (i.e., profiles of increasing density) of approximate Arctic form (i.e., salinity always increasing with depth and temperature initially increasing and then decreasing with depth), one (labeled A) warmer and saltier than the other (labeled B). Our hypothesis is that, unless vertical motion is large, the θ-S zigzags generally form within the envelope of these two curves. This is motivated by simple conservation/mixing arguments.

[26] Consider firstly mechanical mixing (i.e., straight line mixing in θ-S space). For profiles of the form of Figure 3b, any linear mixing between a point on profile A and a point on profile B gives a resultant that lies below (i.e., is colder and/or fresher than) profile A. For starting points close in density (isopycnals marked as dashed lines) the resultant mixing line also lies above (i.e., is warmer and/or saltier) than profile B, and thus the mixing product is enclosed by the envelope of the two parent profiles. Note that diapycnal mixing of two parcels of water of widely differing densities may create a water that lies outside the envelope of the two water columns, as illustrated by points MA and MB (parents) and MM (equal parts mixing product) in Figure 3b. This, however, requires the two starting products to have very different densities, implying in the generally weakly stratified Arctic, the unlikely scenario of a mixing between very different water depths without involving waters in between.

[27] Consider now double diffusive mixing. Here especially it is required that initial densities are similar. Even if one assumes temperatures equilibrate and salinities remain distinct, the resultant (assuming equal volumes) lies within the envelope of the two parent water columns (see points DA, DB and arrows). Note that even if the volumes are not equal, final temperature and salinities are still almost always within the envelope of the parent water columns and certainly (as discussed above) confined to be less than the profile maximums of temperature and salinity, and greater than the profile minimums of temperature and salinity.

[28] Thus, we conclude, any mixing of these water columns gives a resultant lying generally within the envelope of the original parent water columns.

[29] Figures 3c and 3d indicate schematically possibilities for the combination of the two water columns, assuming (for simplicity) a 1:1 volume mixing. An isopyncal mixing would result in one smooth profile midway between the two original profiles, as in Figure 3c. In contrast, the double diffusive process would result in interleaving of layers of water resulting in zigzags in θ-S space (Figure 3d), with the angles of the zigzags being fixed by double diffusive theory. One possibility is for the points of the zigzags to lie on the original water column profiles. This implies the cores of the layers are unaffected by the diffusion processes and maintain their original characteristics. This is the simplest form of slantwise convection [*Walsh and Carmack*, 2003]. In this case the amplitude of the zigzags in θ-S space indicates the difference between the parent water masses. A second possibility is that mixing/diffusion acts throughout the layer, resulting in an erosion of the peaks in θ-S space, as illustrated in Figure 3e. (Note that, as in the inset to Figure 3e, this mixing may erode the peaks with little

change to the separation of the zigzags in density space.) In this case, the amplitude of the zigzags in θ-S space is less than the difference between the parent water masses.

[30] Also note that since the angles of the zigzags in θ-S space are fixed by double diffusive theory (and indeed observations), this implies that the spacing of the zigzag peaks in density space (i.e., the number of zigzags between isopycnals) is related to the initial difference between the two parent water columns. For example, where water column differences are large (e.g., near the temperature maximum as drawn, labeled "Big" in Figure 3d) the zigzags will be large and the peaks far apart in density space, whilst in contrast where the water column differences are smaller (e.g., towards the denser, higher salinity portion of the schematic water columns, labeled "Small" in Figure 3d, and also everywhere in Figure 3f) the zigzags will be small and thus the peaks closer together in density space.

[31] Consider too the final state of these structures in the ocean. Mechanical mixing may act to erode away the peaks. This will not make a significant change to the spacing of the peaks in density space, merely erode them as seen in Figure 3e. Also, given that theory suggests a large-amplitude steady state for the intrusions, it seems unlikely that the large scale zigzags will cascade down into smaller scale zigzags. Note finally that the Arctic Ocean general circulation is generally believed to be a low energy environment - the circum Arctic Boundary Current is order a few cm/s and interior flows (apart from eddies) are weak [*Aagaard*, 1989; *Woodgate et al.*, 2001]. Thus, other than in particular regions (e.g., near inputs to the Arctic, especially near the Barents Sea) little energy is available for turbulent mixing, and it is plausible that θ-S structures may advect

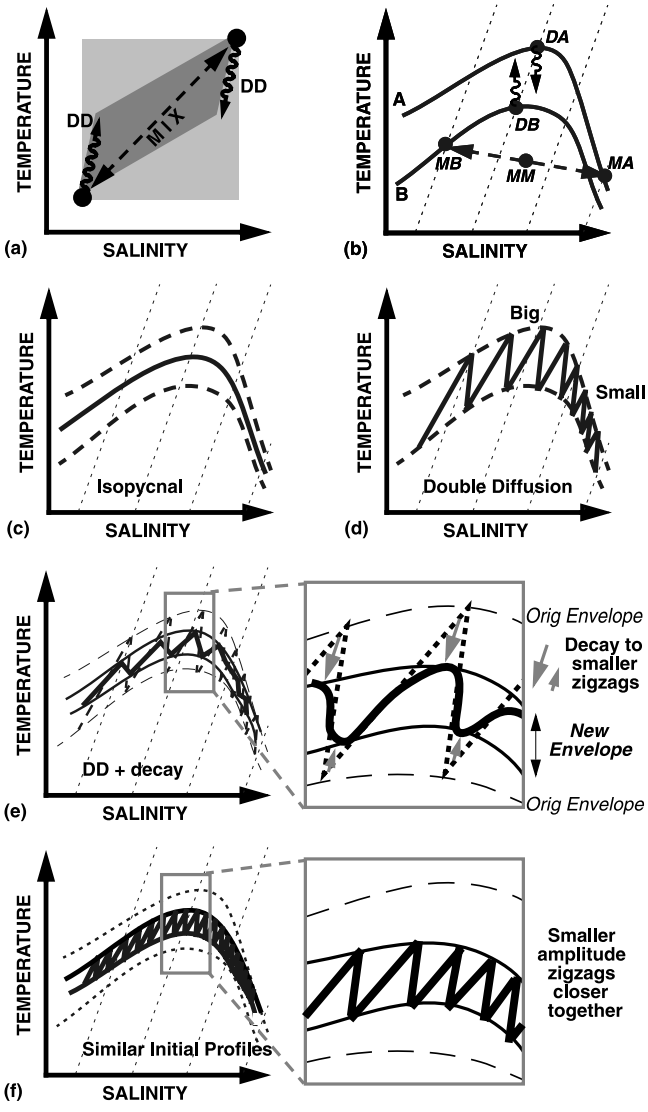

Figure 3. Schematic of effects of mixing processes in temperature-salinity space, as described in the text. Thin dashed lines represent schematic isopycnals. (a) Starting from two distinct water masses (black dots) in temperature-salinity space, mechanical mixing yields a resultant with water properties lying on a straight line between the parent water masses (dashed line with arrows labeled "MIX"). In contrast, double diffusive processes act to equalize temperature faster than salinity, with a resultant change in temperature-salinity space as indicated by wiggly arrows labeled "DD". A combination of these processes (double diffusion and mixing) allows the resultant water to lie within the dark grey zone (assuming both processes are roughly equally present). Whatever combination of processes act, the resultant cannot lie outside the light grey area. (b) Schematic of the mixing of two distinct water columns, as described in the text. (c) Thick solid line shows the resultant of mixing the two water columns of Figure 3b (shown here as dashed lines) isopycnally in equal quantities. (d) Thick solid zigzag line shows a possible outcome of double diffusive (DD) processes acting on the interface between the two water columns (dashed lines). Note in the region where the difference between the two water columns is larger (here at lower salinities, labeled "Big"), the zigzags are of larger amplitude and the peaks are more spaced in density than in the region where the two water columns are similar (here at higher salinities, labeled "Small"). (e) Thick solid zigzag line shows the hypothetical decay of the structure of the solid line zigzags of Figure 3d (here broken zigzag lines) by small scale vertical mixing. The inset panel (showing details of a portion of the left hand panel), indicates with arrows how mixing can erode the large zigzags to smaller amplitude zigzags. Although the amplitude of the peaks erodes, the spacing of the peaks in density space remains much the same. Thin (smooth) dashed lines mark the original ("orig") envelope of the large zigzags. Thin (smooth) solid lines mark the new envelope of the maximums and minimums of the decayed zigzag structures, and this envelope will be used in Figure 3f. (f) Taking the thin solid lines of Figure 3e as the parent water columns, thick solid zigzag line shows a possible outcome of double diffusive processes acting between these columns. Again, an inset panel shows detail from a portion of the left hand panel. Note that although the zigzag amplitude is the same that of the thick solid zigzag line in Figure 3e, the spacing of the peaks in density space is much smaller. This difference in structures between Figures 3e and 3f allows us to distinguish the initial separation of the parent water masses.

largely unaltered over significant distances, the idea of "fossil" intrusions suggested by several authors.

[32] In summary thus, our analysis leads to some simplistic but useful conclusions:

[33] 1. The θ-S values, amplitude and form of the zigzags give an indication of the θ-S properties of the parent water columns, in particular: the zigzags generally lie within the envelope of the parent water columns, and the spacing of the peaks in density space and possibly the amplitude in θ-S space reflects the separation in θ-S of the parent water columns.

[34] 2. The points of the zigzags contain the least altered water, a conclusion that we will test below using tracer data.

[35] 3. Deviations of the zigzag form from the pure interleaving case could be an indication of diffusive or mechanical mixing processes.

[36] We will now use these conclusions to address the various temperature-salinity structures found in the 2002 data from the CBLMR region, with especial focus on parent water columns and mixing processes.

4.2. Frontal Structures in θ-S at the Northern End of the Chukchi Rise

[37] The colored lines of Figure 4 indicate the θ-S structures found in a section of CTD casts taken over the Mendeleev Abyssal Plain, east of the Mendeleev Ridge and just northwest of the Chukchi Rise. The top panel (with salinities between 34.75 and 34.9 psu) illustrate the θ-S range of both the Fram Strait Branch Water (FSBW) (temperature maximum at salinities around 34.85 psu) and the Barents Sea Branch Water (BSBW) (water with sigma-0 around 28.0 kg/m^3).

[38] The most dramatic zigzags (middle panel) are found in the FSBW. Note the nesting of the zigzags. By our previous discussion, we argue these zigzags represent an interleaving of waters of core θ-S around the peaks of the zigzag i.e., a warm salty layer around 1.15°C, 34.85 psu or warmer/saltier (properties consistent with the 1990s FSBW warm anomaly), and a colder fresher layer around 0.7°C, 34.82 psu or colder/fresher (properties consistent with a warmed version of the traditional waters of the Canadian Basin from the early 1990s [*Melling*, 1998; *McLaughlin et al.*, 2002, 2004]). Thus, we conclude these large zigzag profiles represent an interleaving between the newer, warmer FSBW and the older, colder Canadian Basin water.

[39] Such a distinction should be evident in tracer data, e.g., dissolved oxygen and CFC-11. For example, Figure 5 shows vertical profiles from one station (cast 33 at 80° 14′N, 172° 50′W – black curve of Figure 4) of θ, S and dissolved oxygen obtained as continuous data from the CTD, which suggest that dissolved oxygen is indeed low in the colder, fresher peaks of the zigzag structure, although we note with caution that the dissolved oxygen sensor does have a strong temperature dependence, and the variability seen is not much greater than the estimated uncertainty in the data of $\sim$2 μmol/kg. That said, the continuous oxygen data are confirmed with bottle sample data (also in Figure 5) and the conclusion that the colder, fresher layer is older is also supported by CFC-11 data from the same bottle trips (same figure). Unfortunately, other than at a few lucky exceptions, due to the thinness of the interleaving layers (10–50 m), the vertical resolution of the bottle data from the CBL2002 data set does not generally resolve the interleaving. Usually, within a profile, the continuous oxygen data do concur with separate layers having different oxygen, although the differences are frequently small. More convincing is to consider the entire data set (Figure 6), which shows, in the θ-S regime of the FSBW, the warmer saltier waters have higher oxygen and are thus younger. The same figure also shows CFC-11 bottle data, which lead to the same conclusion. Note that the zigzag structures tend to zigzag between two regimes (compare profiles of Figure 4 with tracer values in Figure 6), supporting the idea that peaks of the zigzags are from differing parent water columns (see Figure 3).

[40] Also dramatic in Figure 6 is the high oxygen and CFC-11 in the colder regime of the BSBW (water with sigma-0 around 28.0 kg/m^3). This θ-S region also exhibits double diffusive zigzags (Figure 4), as first observed by *Carmack et al.* [1998]. The magnitude of the zigzags is much smaller, suggesting the parent water masses were more similar in θ-S (see Figure 3). Here, in contrast to the FSBW, it is the warmer, saltier side of the zigzags that has the lower oxygen and CFC-11 data, suggesting these are the older waters. Reference to prior data [e.g., *McLaughlin et al.*, 2004, Figure 12] shows that the older Canadian Basin waters are in fact warmer and saltier than the newer waters advecting eastward from the Eurasian Basin, and we will use this below to study pathways through the CBLMR region.

[41] The final panel of Figure 4 shows how dramatically the θ-S structures may vary over short distances near the slope. The transition from the clean zigzags of the upper panels to a smoothed profile occurs over a distance of less than 30 km, with stations over the slope (where water depth varies from 2500 to 600 m) separated by only $\sim$3 km exhibiting startlingly different profiles. The smoothness of the shallowest profiles is suggestive of vertical mechanical mixing smoothing the θ-S forms. This is plausible since the slope is a much higher energy environment than the deep basin [see, e.g., *Shimada et al.*, 2004; *Pinkel*, 2005]. Nutrient data (not shown) also indicate some Pacific influence, even down as deep as 300 m, consistent with vertical mixing of Pacific waters down. Certainly, the temperature maximum varies dramatically over this short distance, indicating that in such regions, care must be taken to distinguish between spatial and temporal resolution when comparing stations from separate years.

[42] The approach taken by *Shimada et al.* [2004], to consider the temperature on a sigma-0 surface of 27.9 kg/m^3, masks much of the zigzag structure observed here. Our conjecture that vertical mixing smoothes the zigzags suggests that integrating temperature over a certain depth range might also prove efficacious in providing a smoother spatial field. On the other hand, the θ-S structures themselves contain information which arguably help rather than hinder our understanding of the circulation in the CBLMR region. It turns out that five main structures are required to addresses most of the variability observed during this 2002 cruise.

4.3. θ-S Structures in the Fram Strait Branch Water (FSBW)

[43] Figure 7 shows all the profiles of the CBL2002 cruise, grouped according to geographical location as per

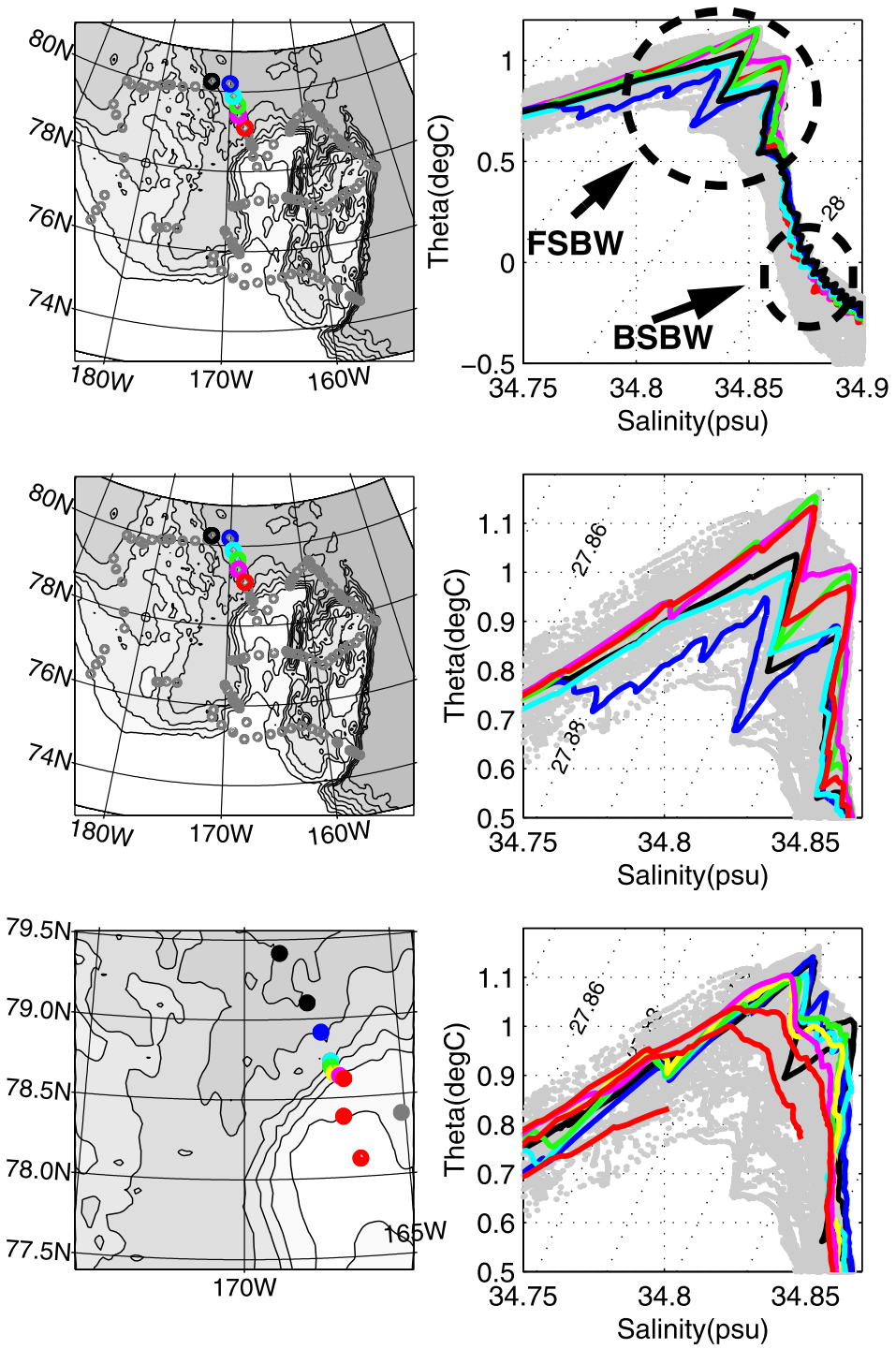

Figure 4. Potential temperature (theta) versus salinity plots for CBL2002 CTD data from the northwest slope of the Chukchi Rise. For θ-S plots (right), grey dots show the entire CBL2002 data set, with locations given by grey dots in the left-hand maps. Oblique dotted lines are sigma-0 isopycnals in kg/m^3. Within each row, individual profiles are marked in color, both on the map and on the θ-S plot. For the maps, depth contours are from IBCAO, at depth interval of 500 m. Note the change of scale in the bottom left-hand panel, which focuses on the northwest edge of the Chukchi Rise.

the inset maps, with color indicating approximate water depth. For example, the second panel in the top row (labeled 35:46) shows data from the section to the northwest of the Chukchi Rise, and contains many of the same profiles as Figure 4, indicating the large zigzag structures in the deeper water (black lines) and the smoother form of the temperature maximum in the shallower water (red lines). A similar transition is seen to the northeast of the Rise (third panel,

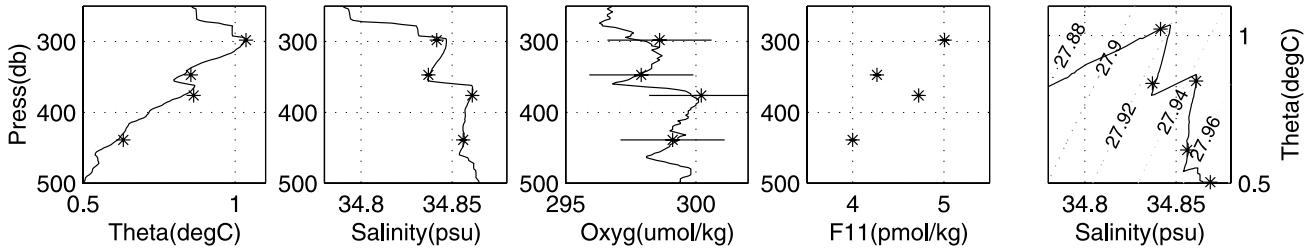

Figure 5. From left to right, profiles with pressure of potential temperature (theta), salinity, dissolved oxygen (oxyg) and CFC-11 for station 33 (80° 14′N, 172° 50′W, black dot and profiles in top two panels of Figure 4) in the Canada Basin. Far right panel shows the same data in θ-S space, with oblique dotted lines indicating sigma-0 isopycnals in kg/m^3. Asterisks denote bottle data, with horizontal lines marking estimated error bars as per section 2. For CFC11, these error bars are too small to be visible on this scale. Errors for profile data are as discussed in section 2, i.e., ~0.002°C; ~0.002 psu; ~1 dbar; <2 μmol/kg (CTD-oxygen, calibrated against bottle samples).

top row, labeled 47:56). The large zigzag structures are only evident in the black and blue lines of top row of the figure, showing these structures are only found in deep water (from the color of the line) and in the north of our study area (see inset map for locations). Similarly, the smoothed temperature maximum is not ubiquitous, but is found only in shallow stations (red, mauve and green lines) and geographically in the center of our study area (bottom two rows of second and third columns).

[44] Although there is much variability, certain forms of θ-S structures occur repeatedly. By inspection (Figure 8) we find the profiles can be categorized (with little ambiguity) into five major forms, which turn out to have characteristic oxygen and CFC-11 properties and to exist in restricted geographical areas. Details of the profiles suggest the formation processes. The five forms (in order of decreasing simplicity) are as follows:

[45] 1. Large zigzag structures (Deep Basin, column 3, Figure 8) located adjacent to the Mendeleev Abyssal Plain and Canada Basin in deep water, distinguished by few, large θ-S zigzags, oxygen around 300 μmol/kg and middle to low CFC-11. By the arguments given in section 4.2, we conclude these are the result of an interleaving of the boundary current water and the older deep-basin water, hence the intrusive features display a large range of temperature and salinity.

[46] 2. Smooth θ-S structures (Slope Influenced, column 4, Figure 8) generally located over or around the Chukchi Rise, distinguished by smooth θ-S form, low oxygen and middle CFC-11 values. These were also discussed in section 4.2. Nutrient (especially silicate) data (not shown) suggest these waters have undergone mixing with shelf waters (see discussion of Pacific ventilation of the lower Arctic halocline by *Woodgate et al.* [2005]) and thus that their oxygen values are low due to intense biological activity over the shelves, not due to long isolation from ventilation with the atmosphere, a conclusion backed by the medium CFC values found for these profiles. The smoothed form of the profiles implies diapyncal mixing, also consistent with a vertical mixing of shelf waters.

[47] 3. Small zigzag structures (New Boundary Current, column 1, Figure 8) located exclusively west of the Mendeleev Ridge, distinguished by many small θ-S zigzags, high oxygen and high CFC-11 values. The high oxygen and CFC-11 data suggest these are the newest FSBW found in our sections, consistent with the waters being supplied via the eastward (cyclonically) flowing Arctic Ocean Boundary Current. Note that the maximum temperatures are about 0.1°C colder than the maximum FSBW temperatures found in the CBLMR region, consistent with the reported cooling of the FSBW that has been found following the original rise in FSBW temperature [*Woodgate et al.*, 2001; *Gunn and Muench*, 2001]. This conclusion also explains the small zigzags, which imply the interleaving of waters with similar θ-S values, i.e., we see here the interaction between the 1990s warm core and the following slightly colder waters, the implication being the older, warmer waters have spread perpendicular to the topography and the newer waters now form the core of the current.

[48] 4. Ragged zigzag structures (Relic Waters, column 5, Figure 8) located within the Northwind Abyssal Plain, distinguished by ragged, comparatively cold θ-S zigzags, low CFC-11 and low oxygen. These profiles are colder in maximum temperature than columns 1 or 3, suggesting these are older waters. Tracer data, especially CFC data, support this view, with CFC-11 values being particularly old in the southern portion of the region. The oxygen values are also lower than in regions to the west, with the exception of the Slope Influenced stations (column 4), which have extremely low oxygen due to biological activity. The implication is that this region is poorly and slowly ventilated from the boundary current and contains older Canadian Basin waters, which in the temperature maximum core was colder and fresher than the FSBW of the 1990s.

[49] 5. "Point-and-bump" zigzag structures (Boundary Current, column 2, Figure 8) located over the slope both around Chukchi Rise and the Chukchi Abyssal Plain (the comparatively deep region between the Chukchi Rise and the Mendeleev Ridge), distinguished by a slightly smooth, double peak structure in θ-S space, high CFC-11, moderately high oxygen, and high core temperatures. These profiles generally coincide with the highest temperature, oxygen and CFC-11 values within a section across the slope, and thus are assumed to be the core of the boundary

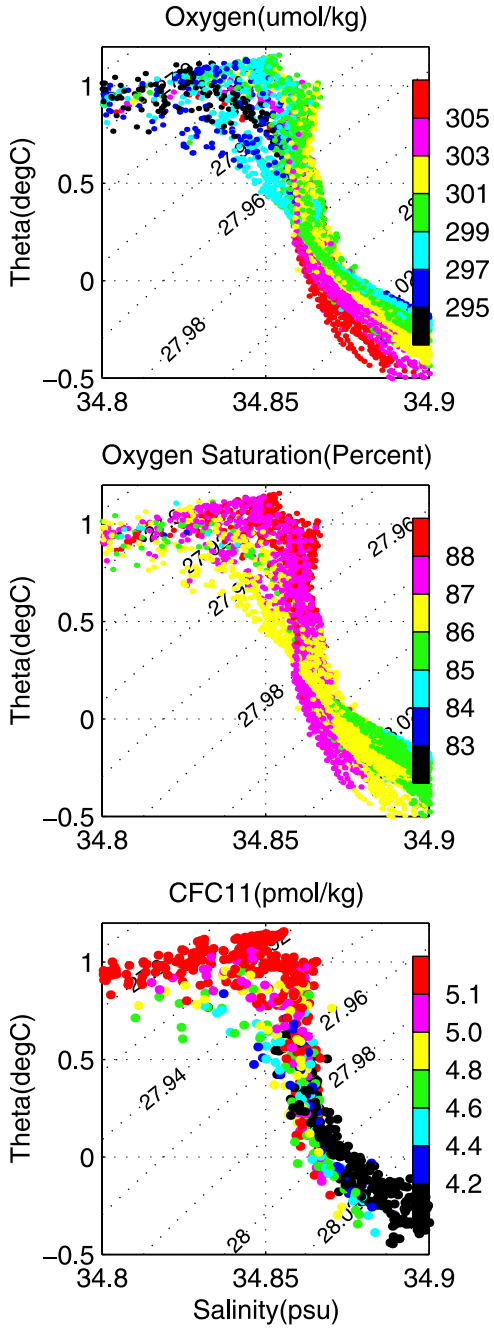

Figure 6. Scatterplots of potential temperature (theta) against salinity for the CBL2002 data set for (top) CTD data colored with CTD-oxygen; (middle) CTD data colored with oxygen saturation; and (bottom) bottle data colored with CFC-11. Note that for clarity only 1/10th of the 2 db CTD data are used for the top two plots.

current, marking the progression of the FSBW warming anomaly of the 1990s through the CBLMR region. The "point-and-bump" structure, generally smoother than the zigzag form, is also consistent with being near the core of the current, since we expect the core of the current to be (i) less modified by the double diffusive structures than the edges of the current, and (ii) to have higher velocities and thus presumably greater turbulent mixing than the edges of the current. These structures are found over isobaths from ~600 to 3000 m, predominantly between the 1500 to 2500 m isobath, consistent with the isobath of the boundary current near the junction of the Lomonosov Ridge and the Eurasian continent [*Woodgate et al.*, 2001].

[50] Thus, different θ-S forms maybe used to trace different parts of the boundary current. We note in particular, that the point-and-bump structure might be used to denote the core of the current in situations when other tracers are not available.

4.4. θ-S Structures in the Barents Sea Branch Water (BSBW)

[51] The complete set of θ-S structures of Figure 7 also shows a variety of structures in the Barents Sea Branch Water (BSBW) and the deeper waters. Figure 9 shows θ-S, oxygen and CFC-11 values for the deeper part of the water column, using the same groupings as in Figure 8. With the exception of one group (the Slope Influenced waters of column 4), to a large extent these groupings also successfully categorize the BSBW and deeper waters into different property and geographical regimes. This suggests different depths of flow are experiencing much the same circulation pathways.

[52] Broadly, the BSBW and deeper waters may be categorized into four types, namely:

[53] 1. Warm zigzag structures (Deep Basin, column 3, Figure 9) located in the deep waters adjoining the Mendeleev Abyssal Plain and Canada Basin, also characterized by medium oxygen and medium/low CFC-11 (same stations as the big zigzags of the FSBW). The clear interleaving structures here are again consistent with the interaction of the boundary current waters with the older waters of the Canadian Basin, albeit over a deeper set of θ-S. This time, in contrast to the FSBW, the older basin waters are warmer and saltier than the boundary current waters.

[54] 2. Cold zigzag structures (New Boundary Current, column 1, Figure 9) located exclusively west of the Mendeleev Ridge, also characterized by high oxygen and CFC-11 (same stations as the small zigzags of the FSBW). The clear interleaving again suggests the interaction of the boundary current waters with older, interior basin waters. Again, tracer values show these to be the newest waters at this depth range within our data set, consistent with supply of the boundary current waters from the west. Note also, that this newest BSBW is fresher and colder than any of the other BSBW found in this data set.

[55] 3. Smooth, warm, low oxygen θ-S structures (Relic Waters, column 5, Figure 9) located over the Northwind Abyssal Plain, (same stations as the ragged θ-S profiles of the FSBW). Just as for the FSBW profiles in this region, the low oxygen and CFC-11 values for the BSBW profiles suggest poor ventilation for this area. Note, however, that two profiles of this group have anomalously lower temperatures and higher oxygen and CFC-11 than the rest of this group. These lie on the east side of the Chukchi Rise and the east side of the Northwind Ridge, and may indicate the intrusion of boundary current waters in from the north. We will return to this in section 5.2.

[56] 4. Smooth, cooler θ-S structures (Boundary Current, column 2, Figure 9) located over the slope around the

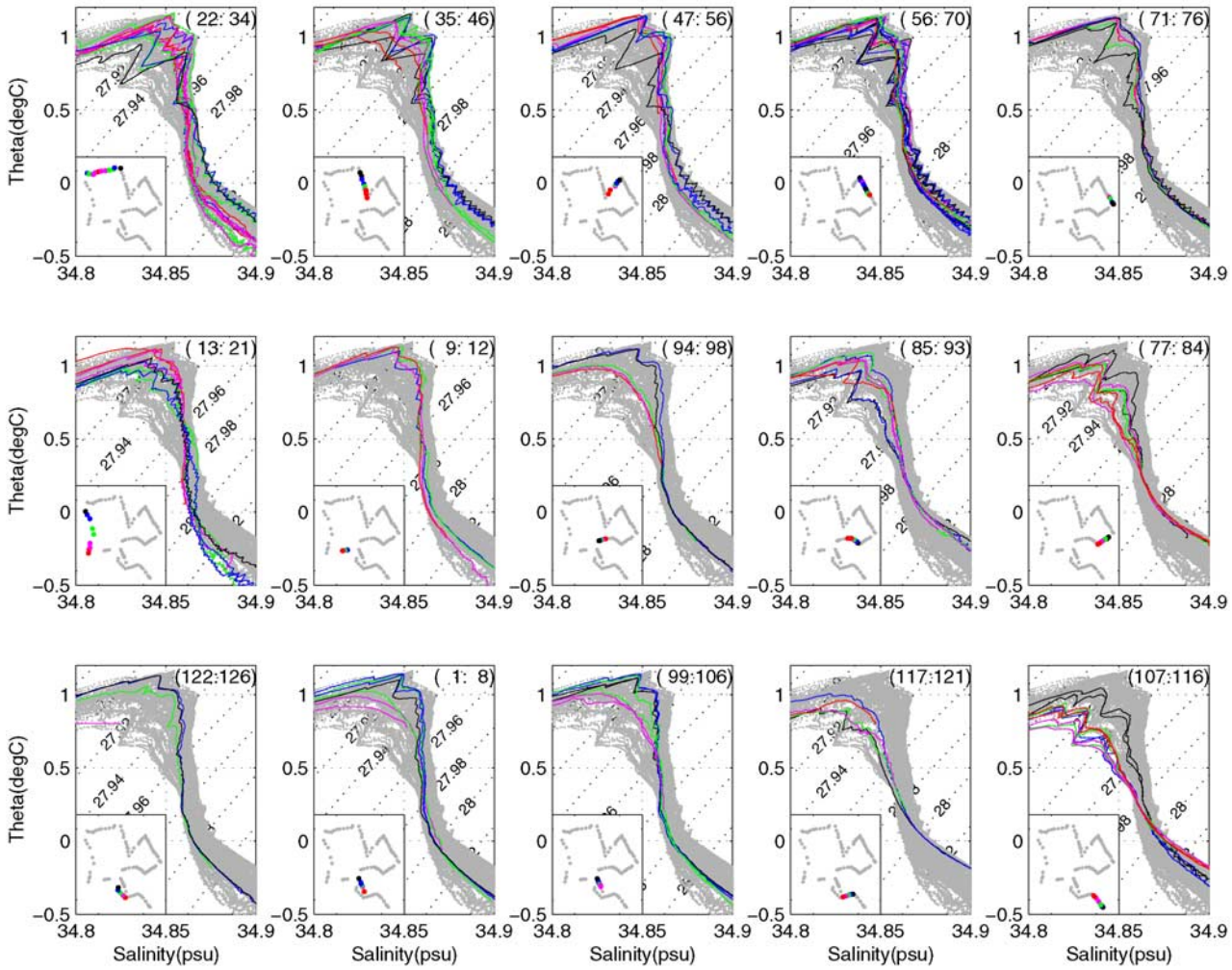

Figure 7. Potential temperature (theta) versus salinity plots for CBL2002 data set. Oblique dotted lines are sigma-0 isopycnals in kg/m^3. In each panel, grey indicates the entire data set, with colored lines representing various profiles from locations shown schematically in the inset map. Color indicates approximate water depth, with black being deep and red being shallow. The range of stations numbers used for each panel is labeled in the top right of each panel. Panel layout represents geography of the region. For example, sections from north of the study zone are on the top row of the figure, and stations from the west are on the left-hand side of the figure. See section 4.3 for discussion.

Chukchi Rise and the Chukchi Abyssal Plain, with medium values for oxygen and CFC-11 (same stations as the smoothed zigzag profiles of the FSBW). By the same arguments used above, we assume these profiles mark the core of the boundary current.

[57] The fourth column of Figure 9 corresponds to the smoothed θ-S structures in the FSBW, which are hypothesized to be influenced by shelf mixing processes. One might assume these processes only influence the upper few hundred metres - most of the profiles are in shallow regions - and thus profiles in this category belonged originally in one of the other four categories (depending on geographical location), before being altered by shelf mixing. Indeed, the few profiles that are deep enough to extend to the BSBW (column 4, Figure 9) do show differing water properties, and may be classed in columns 2 and 5 (Boundary Current and Relic Waters). In each case, this categorization is consistent with their geographical location.

5. Atlantic Water Circulation Through the Mendeleev Ridge and Chukchi Borderland Region

[58] Our best understanding of the Atlantic water circulation through the Mendeleev Ridge and Chukchi Borderland region (CBLMR) draws on the information gained from the θ-S zigzag structures, results from oxygen and tracer data, and an understanding of the physical mechanisms by which the Atlantic water propagates.

[59] Previous studies have noted that the boundary current tends to follow topography [*Rudels et al.*, 1994]. Since the current is dominantly barotropic, this is most simply explained by conservation of potential vorticity. In this case, signals are advected along f/H contours (f = Coriolis

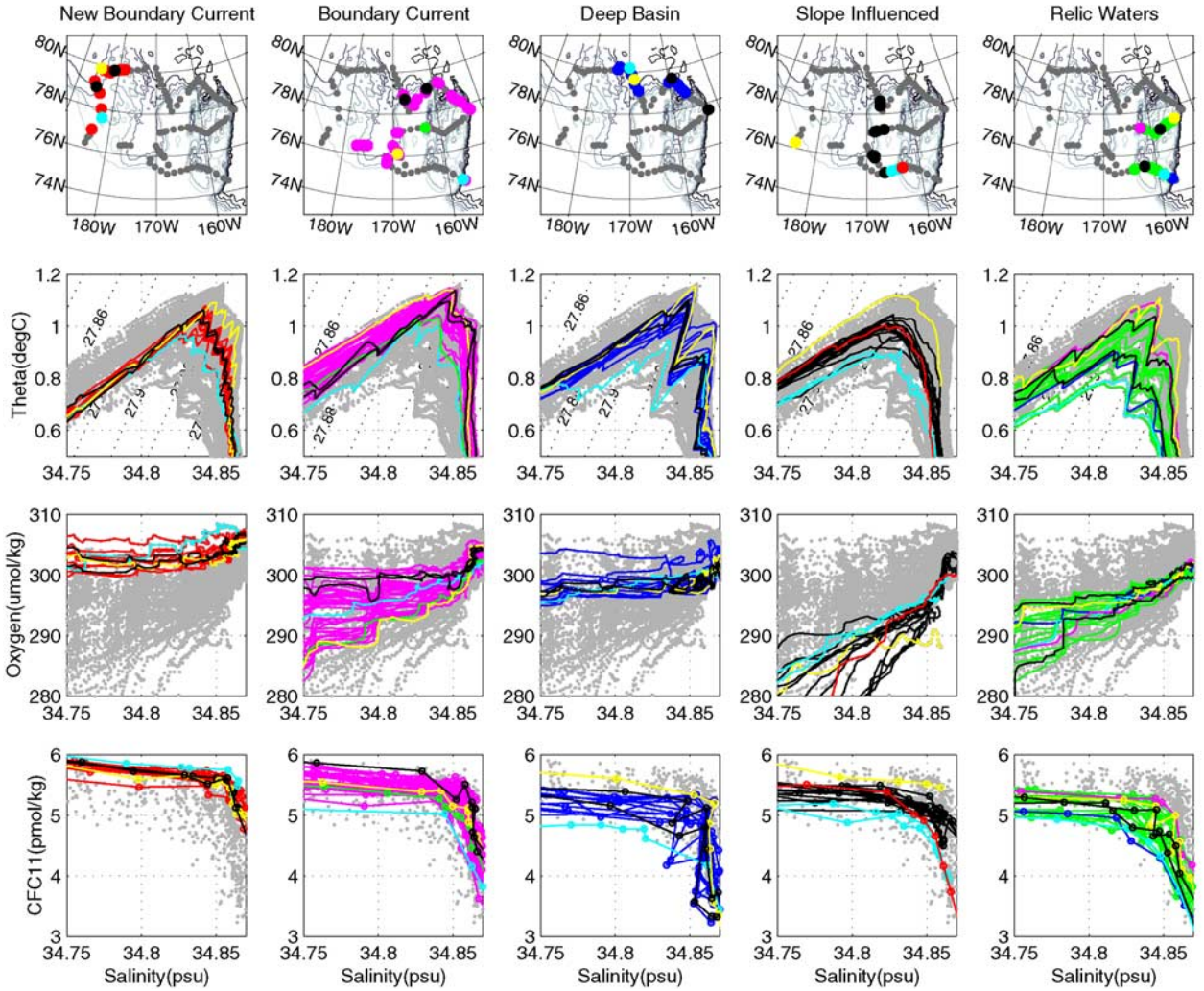

Figure 8. Composite plot of location (top row); potential temperature (theta) versus salinity (second row); CTD oxygen versus salinity (third row); and CFC-11 versus salinity (fourth row) for the CBL2002 data in the property regimes corresponding to the approximate depth range of the Fram Strait Branch Water (FSBW). See section 4.3 for discussion.

parameter; H = water depth). For the Arctic where f varies little, these contours are very similar to isobaths, and we expect the boundary current to follow slopes and ridges as has been observed in the Eurasian Basin. In the CBLMR region, especially over the Mendeleev Ridge and the Northwind Abyssal Plain, the sea floor topography is convoluted and still poorly mapped. In slope regions, seafloor gradients observed on the CBL2002 cruise were frequently much sharper than depicted by the best available bathymetry (IBCAO, International Bathymetric Chart of the Arctic Ocean [*Jakobsson et al.*, 2000]), with discrepancies being up to 1000 m over short distances. It is not clear what topographic valleys exist through the Mendeleev Ridge, and details of the Northwind Abyssal Plain, the Northwind Ridge and the northern edge of the Chukchi Rise are still unresolved. Thus, although we use the IBCAO bathymetry as an aid to understanding circulation patterns, we must also admit the possibility of topography that is uncharted.

[60] In general, advection speeds are slow in the Arctic and have been measured at ~5 cm/s on the Eurasian continental slope west of the Lomonosov Ridge and ~2 cm/s on the Eurasian continental slope east of the Lomonosov Ridge [*Woodgate et al.*, 2001]. For scale, recall that a 2 cm/s current corresponds to ~600 km a year (~6 degrees of latitude, or ~20 degrees of longitude at 75°N). These speeds (measured by current meters) are consistent with the advection of temperature signals along the continental shelf [*Woodgate et al.*, 2001]. (Since at low temperatures density is primarily a function of salinity not temperature, it is only a small simplification to consider temperature as a primarily passive tracer in the Arctic.)

[61] The double diffusive interleaving processes also induce velocities, but theory suggests these velocities are perpendicular to the front, i.e. here across isobaths [*McDougall*, 1985a]. In any case, a combination of theory and observations estimates the spreading speeds at ~1–2 mm/s, an order of magnitude less than the along-slope

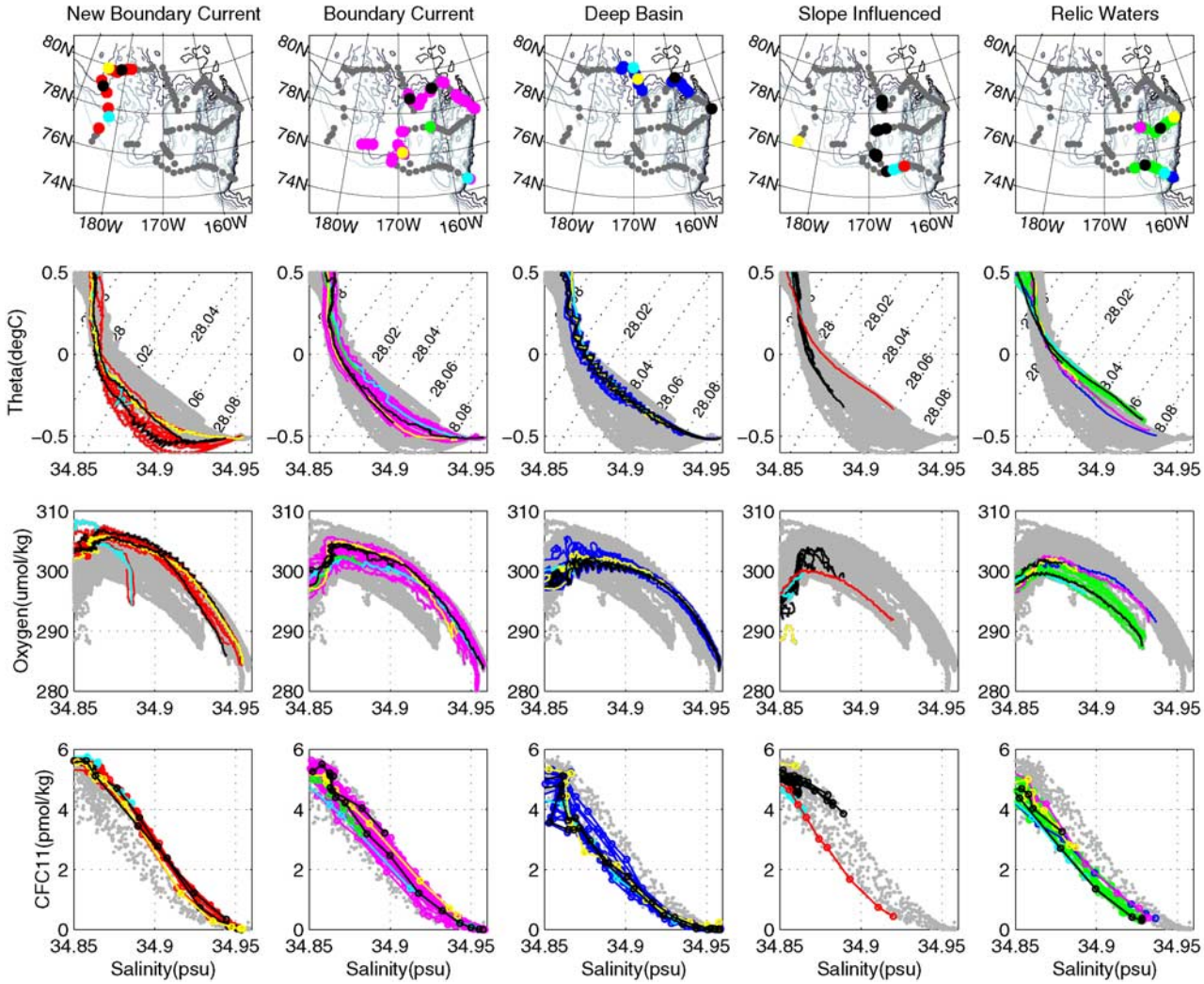

Figure 9. Composite plot of location (top row); potential temperature (theta) versus salinity (second row); CTD oxygen versus salinity (third row); and CFC-11 versus salinity (fourth row) for the CBL2002 data in the property regimes corresponding to the approximate depth range of the Barents Sea Branch Water (BSBW) and the deeper waters of the Arctic Ocean. See section 4.4 for discussion.

advective speed. A speed of 2 mm/s is equivalent to ~60 km a year (~0.6 degrees of latitude or ~2 degrees of longitude at 75°N) and thus, in a year, this double-diffusive spreading is comparable to the order 50 km width of the boundary current [*Woodgate et al.*, 2001].

[62] Transferring the along-slope velocities to the CBLMR region indicates that a current advecting at this speed would take many years to traverse the region, with the time depending on the isobath it follows. For example, the route from the southern Chukchi Abyssal Plain (starting from northeast of Herald Canyon) to the southern foot of the Northwind Ridge varies from ~1400 km along the 1800 m contour (which lies north of both the Chukchi Rise and the Northwind Ridge), to ~1200 km along the ~1000 m contour (north of the Chukchi Rise, but south of the Northwind Ridge), to ~600 km along the 600 m contour (south of both the Chukchi Rise and the Northwind Ridge, the "Chukchi Gap" route suggested by *McLaughlin et al.* [2004] and *Shimada et al.* [2004]). At 2 cm/s, these distances correspond to travel times of ~800 days, ~700 days and ~350 days. Even in this simplest construction, the passage of the boundary current through the Chukchi Borderland introduces a large temporal phase shift between different parts of the current, so that when the different trajectories recombine east of the Chukchi Borderland, the boundary waters carry a time history of the upstream flow integrated over several years. Similar considerations apply to the region of the Mendeleev Ridge.

[63] A consideration of Figure 2 shows it is extremely difficult to test this hypothesis with the data currently available. For example, although we may conclude that the region north of the Chukchi Rise warmed at some stage between 1996 and 1998, one point is insufficient to assess the speed of advection of the warming, without clear temporal information on the temperature variability entering the CBLMR region (information that we lack this far downstream of the Atlantic water entrance to the Arctic). Thus, given the variable sampling from year to year and the

sizeable spatial variability of the field we are measuring, it is hard to be precise on advective timescales. Yet, it is clear that the warming passes into most of the CBLMR region over a period of several years, implying advective speeds of order 1–2 cm/s.

5.1. Structure and Changes in θ-S Properties of the Boundary Current

[64] The multiyear pathways through the CBLMR region indicate that the 2002 snapshot of water properties in the region actually show a time history of the properties of the boundary current. Using CFC-11 (and to some extent oxygen) data to distinguish the relative ages of waters in the CBL region, we can infer a time history of the θ-S properties of the boundary current, and understand some of the spatial variability in the CBLMR region as the advection of a time-varying signal (Figure 10).

[65] We have seen above, that the newest FSBW in our data is not the warmest FSBW, suggesting that in 2002 within the Atlantic water temperature maximum core, the cooling that follows the dramatic warming of the FSBW has traversed as far as the Mendeleev Ridge. This cooling had not yet, however, reached east of the Mendeleev Ridge, and thus, for the Chukchi Borderland region of our domain, high FSBW temperatures still correspond to the newest water locally. Within the Chukchi Borderland region we find both the warm FSBW and the older, colder temperature maximum waters. Thus in total, within the CBL2002 data we see three regimes of the core temperature maximum of the FSBW. The oldest FSBW is coldest, the middle-aged water is warmest and the newer water is cooler than the middle-aged water (Figure 8). Similarly, we find three types of BSBW, as illustrated in Figure 9. Here, however, the oldest water is the warmest, the middle-aged water is colder, and the newest water is the coldest yet.

[66] Especially interesting here is that the different regimes agree geographically. This implies the flow structure is at least equivalent barotropic in the vertical over this portion of the water column (i.e., within a water column, the flow has the same direction, if not necessarily the same speed). This vertical structure has been measured in the boundary current near the Lomonosov Ridge, where the speed was found to decrease with depth. This in turn implies that the BSBW may take significantly longer to propagate through the CBLMR region than the FSBW.

[67] Figure 10 plots CFC-11 at various depth levels. Both at 375 dbar and 700 dbar, the CFC-11 values are highest in the west, consistent with the newest waters being supplied by the cyclonic boundary current. Around the Chukchi Rise, the highest values are over the slope, marking the core of the current. North and east of the Chukchi Rise, the high spatial variability reflects the underlying topography. The same patterns are seen in the oxygen data, here averaged from 600 to 1000 dbar. If the flow difference between the FSBW and the BSBW were large, then one would expect at the deeper levels there to be a greater range of CFC-11 values between the newest and the oldest waters. There is little strong evidence of this in Figure 10: the difference between the Mendeleev Ridge and the northeast end of the Chukchi Rise is perhaps a little greater in the deeper waters; however, a proper analysis here requires a careful consideration of source and mixing function, preferably backed by further tracer data and is beyond the scope of this paper.

[68] The θ-S interleaving analysis allows us to draw some conclusions about the width of the current. As is seen in Figure 8 (column 4), the inshore side of the current is frequently influenced by shelf processes. This influence can affect the boundary current over isobaths of at least 1000 m, sometimes 1500 m. In the sections that extend northwards towards the deep Canadian Basin, the large interleaving between the boundary current and the interior waters occurs always over isobaths deeper than 3500 m, and sometimes over 3000 m or even 2500 m. Thus, most generally the boundary current is found over the slope between approximately 1000 or 1500 m and 2500 or 3500 m. In the sections taken, water properties suggest a width of order 50 km for the current, consistent with the width estimated around the Lomonosov Ridge [*Woodgate et al.*, 2001].

[69] Very striking is the link of water properties to topography, especially at the north end of the Chukchi Rise, where even moderate changes in bottom depth (from 3400 m to 3000 m) are reflected in the overlying water properties. For example, in Figure 10, the structures in CFC-11, mean temperatures and oxygen in the northern line at 160°W is related to the section crossing over a topographic rise connected to the northeast point of the Chukchi Rise. This agrees well with the strong link between topographic slope and velocity remarked upon by *Shimada et al.* [2004].

5.2. Pathways of the Boundary Current Through the CBLMR Region

[70] Finally, we use the combined analysis to address the pathways of Atlantic water through the CBLMR region. A schematic of the circulation is given in Figure 11, which also summarizes the θ-S structures and properties discussed above. Whilst a general eastward, bathymetry-following transportation of Atlantic waters is a clear conclusion of this work, there are detailed features which warrant further discussion.

5.2.1. Stagnation and Ventilation of the Northwind Abyssal Plain

[71] Dramatic in these data is the region of relatively isolated water in the Northwind Abyssal Plain. This is evident in the tracer and θ-S data of column 5 (Relic Waters) of Figures 8 and 9. Being bounded to the south by the Chukchi slope, to the east by the Northwind Ridge, to the west by the Chukchi Rise, and to the north by an unnamed ridge of similar magnitude (all these topographic features are ~1000 m or shallower), this ~2000 m deep plateau is topographically isolated, and potential vorticity constraints would suggest a semi-trapped water column in the manner of a Taylor column. The weak stratification (thus predominantly barotropic nature) of the Arctic Ocean allows deep topography to influence the flow structure throughout the water column. Although the waters of this region are distinct to those outside, obviously some slow transfer must occur since the temperature maximum core is still warmer than the decade old Canadian Basin waters [e.g., *McLaughlin et al.*, 2004]. Within the Abyssal Plain, CFC-11, mean temperatures and oxygen (Figure 10) are greatest in the northern part, suggesting the ventilation is provided from the north. This is supported by two profiles at ca. 77°N, east of the Chukchi Rise (magenta in column 5 of

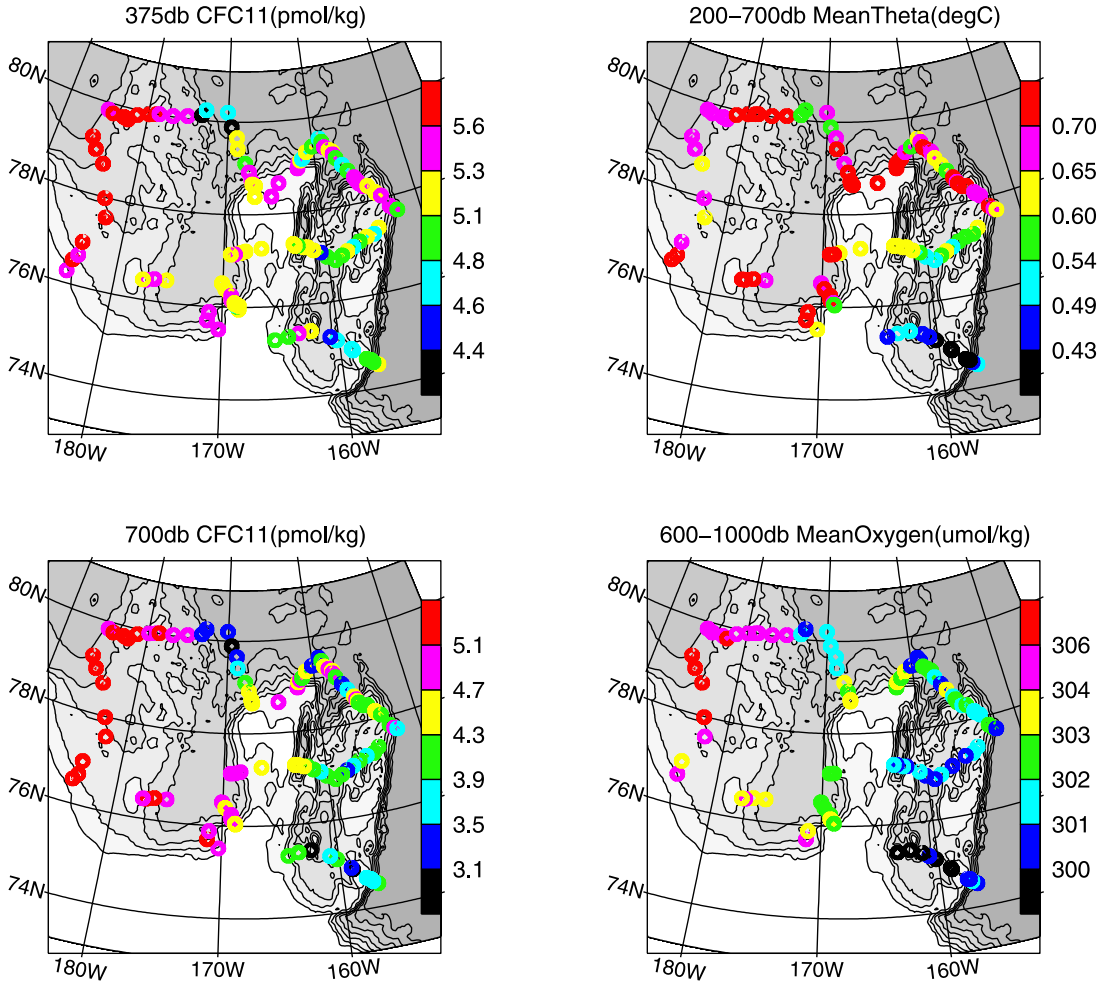

Figure 10. CBL2002 data showing for each station (top left) CFC-11 value linearly interpolated onto the pressure surface of 375 db; (bottom left) CFC-11 value linearly interpolated onto the pressure surface of 700 db; (top right) mean potential temperature (theta) averaged between 200 and 700 db; and (bottom right) mean CTD oxygen averaged between 600 and 1000 db. (Note that the eastmost station of our data is outside the boundary current and thus cooler and lower in CFC-11 and oxygen than its neighbors, and that due to the order of plotting, this data point partially obscures the higher values in adjacent stations.)

Figures 8 and 9), which show the warmer FSBW temperature maximum (Figure 8) and the colder deeper layers (Figure 9) typical of the boundary current. This water may have been part of the boundary current steered topographically around the Chukchi Rise. One other profile from further east (yellow in column 5 of Figures 8 and 9) shows similar properties, raising the possibility that the ventilation may occur through numerous gaps in the topography.

[72] Curiously, our data do not clearly show the southern ventilation pathway suggested by *McLaughlin et al.* [2004] and *Shimada et al.* [2004], i.e., that which enters through the Chukchi Gap and passes along the southern side of the Northwind Abyssal Plain. Although CFC-11 values suggest some higher values in this region (Figure 10, top left panel), stations closer to the slope have lower CFC-11. It is possible that our station spacing of ~25 km may have missed a narrow version of the boundary current, however, even in this case one would expect some signal of the boundary current in the adjoining stations. In fact, the mean temperatures are low on this route (Figure 10, top right panel), and the structure in the temperature maximum layer suggests either the slope influence (light blue profiles in column 4, Slope Influenced, Figure 8) along the section over water depths of 1400 m or less and the older relic waters at greater water depths (column 5, Relic Waters, Figure 8). The distinctive "point and bump" temperature maximum is missing from this section entirely. Within the deeper layers, the water column profiles again resemble the older waters (column 4, Slope Influenced, and column 5, Relic Waters, Figure 9). The IBCAO bathymetry suggests that the sill depth of the Chukchi Gap is between 500 and 1000 m. As discussed above, the warm core of the boundary current lies over deeper water in our data. In our two sections at ca. 76°N, 170°, just west of the Chukchi Gap, over water depths of 1000 m and shallower, the temperature maximum is lower, and oxygen and CFC-11 values are lower than over the deeper water. Two moorings deployed for one month during the CBL002 cruise in this region (76° 1.5′N

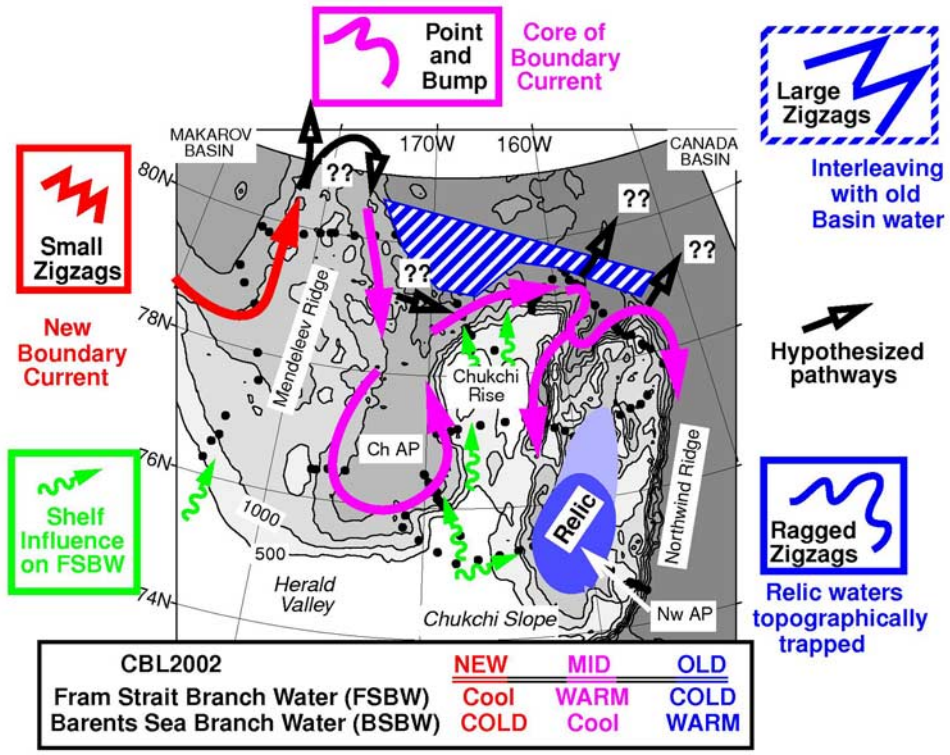

Figure 11. Schematic of Atlantic water circulation in the CBLMR (Chukchi Borderland and Mendeleev Ridge) region of the Arctic Ocean. The newest boundary current waters (red, entering in the west) exhibit small zigzag structures in temperature-salinity space (red arrows and inset schematic). Here the FSBW (Fram Strait Branch Water) is slightly cooler than the maximum observed in the CBL2002 data, but the BSBW (Barents Sea Branch Water) is the coldest found in the CBL2002 data (bottom panel). Black hollow arrows by the Mendeleev Ridge indicate that the boundary current, in some unspecified way, traverses along and somewhere crosses the Mendeleev Ridge. East of the Mendeleev Ridge, the core of the boundary current is marked by a "point and bump" structure in temperature-salinity space (magenta inset schematic). The pathway of the boundary current, firstly south of the Chukchi Abyssal Plain ("Ch AP") and then north and east along the edge of the Chukchi Rise, is indicated with magenta arrows. In these waters the FSBW has its maximum temperatures, while the BSBW is slightly warmer than the newer BSBW to the west (bottom panel). Beyond the northern point of the Chukchi Rise, two pathways are evident in our data - one follows topography to the north of the Northwind Ridge and then turns south; the second follows the eastern flank of the Chukchi Rise southwards. The isolated "relic" waters of the Northwind Abyssal Plain ("Nw AP") are marked here in blue (blue inset panel for "ragged zigzags"), with the northern part of the plain (light blue shaded region) being better ventilated than the southern part of the plain (dark blue shaded region). The large zigzags (striped blue region and inset schematic) are found to the north of the Chukchi Rise, where the boundary current interleaves with the older, colder basin waters. Green wiggly arrows indicate regions where shelf processes affect the FSBW Atlantic water layer. Black hollow arrows north and west of the Chukchi Rise show hypothesized transport from the boundary current into the deep basin and a possible shortcut from the eastern Mendeleev Ridge to the Chukchi Rise. These routes are not confirmed or denied by the present paper. Note that the proposed shelf route through the Chukchi Gap is not marked here, since the CBL2002 data do not show the warm, "point and bump" boundary current taking this route.

168° 31.8′N and 76° 3.1′N 168° 51.0′N) in 626 m and 1090 m of water respectively indeed show the Atlantic water layer over these water depths to be moving westward rather than eastward. Slightly further north (76° 7.8′N 168° 59.2′N) in 1617 m of water, moored measurements from the Atlantic water layer for this same month shows a modest eastward flow. Our data suggest thus that, at least at this time, any flow through the Chukchi Gap carries predominantly shelf influenced waters and not the main core of the current.

5.2.2. Route of the Boundary Current Around/Over the Mendeleev Ridge and Around the Chukchi Borderland

[73] Figures 8, 9 and 10, summarized in Figure 11, illustrate the main topographically steered pathway of the boundary current. They show the current to have crossed the Mendeleev Ridge, and to loop south around the Chukchi Abyssal Plain and north around the Chukchi Rise. There are

still, however, ambiguities in the exact pathways of the flow.

[74] The pathway across the Mendeleev Ridge is still uncertain. There is a clear distinction in properties and ventilation between the two sides of the ridge. At 80°N, where our section crosses the Mendeleev Ridge, the topography is complex. This is typical of the profile of the ridge. Presumably, there exist many potential routes for waters through the ridge [cf. *Swift et al.*, 1997]. Yet, there is a clear distinction in water properties and ventilation between the two sides of the ridge, which would be consistent with the main crossing of the ridge occurring further north than our section. This issue will become clearer when/if more recent data indicate if the cooler zigzag structures cross the ridge.

[75] CFC-11, θ-S structures and oxygen all suggest there is a route for the boundary current between the Mendeleev Ridge and the Chukchi Rise around the southern side of the Chukchi Abyssal Plain. This, however, does not rule out a shortcut of the boundary current from the east side of the Mendeleev Ridge due east over to the Chukchi Rise. Such a shortcut might explain some of the structures found on the northern side of the Chukchi Rise, and would imply that waters at the northwest tip of the Chukchi Rise were better ventilated than those at the south of the Chukchi Abyssal Plain. The properties illustrated in Figure 10 are not definitive on this issue - CFC-11, temperature and oxygen are if anything generally slightly less at the northwest tip of the Chukchi Rise, implying either that the main route is to loop south around the Chukchi Abyssal Plain or that the shortcut route is actually not significantly quicker.

5.2.3. Fate of the Boundary Current After the Chukchi Rise

[76] A matter of debate is the fate of the boundary current waters after the Chukchi Rise, since tracer measurements suggest some mass transfer from the boundary current to the interior basin at these points [*Smith et al.*, 1999; *Smethie et al.*, 2000]. This could occur through eddy shedding from the boundary current, if for example, the topography turns sharper than the Rossby Radius ($\sim$8 km in this region) or a critical angle depending on the vorticity distribution upstream [*Bormans and Garrett*, 1989; *Stern and Whitehead*, 1990; *Klinger*, 1993].

[77] As mentioned above, our data show the boundary current tightly locked to the topography in this region. Boundary current profiles with the warm FSBW core are found at the north end of the Northwind Ridge including on the eastside of the ridge (column 2 of Figure 8) and the lower layers show some interleaving between the oldest and the middle-aged waters (column 3, Figure 9). Figure 10 shows that temperatures, CFC-11 values and oxygen values are higher at the northern end of the Northwind Ridge than at the southern end of the ridge. (Note that the eastmost station of our data is outside the boundary current and thus cooler and lower in CFC-11 and oxygen than its neighbors, and that due to the order of plotting, this data point partially obscures the higher values in adjacent stations.) Thus we conclude at least part of the boundary current has rounded the tip of the Northwind Ridge in 2002 (see also Figure 10). It is equally clear that the temperature maximum has not yet reached the southern part of the Northwind Ridge where core temperatures are still colder and oxygen and CFC-11 values lower than further to the north.

6. Conclusions

[78] The purpose of this paper is to describe the pathways and transformations of the Atlantic water layers in the region of the Mendeleev Ridge and Chukchi Borderland (CBLMR) in 2002, with a particular focus on the Arctic Ocean Boundary Current in this area. To do this we draw on not only core and integrated θ-S properties and tracer data, but also use the structure of temperature-salinity double-diffusive intrusions, zigzags, of the Atlantic waters to help understand the physical system.

[79] Conservation and mixing arguments are used to show that the magnitude, spacing and form of the zigzags in θ-S space include information about the parent water masses from which the intrusions are formed. In particular, the zigzags generally lie within the envelope of the parent water columns; and the spacing of the peaks in density space and possibly the amplitude in θ-S space reflects the separation in θ-S of the parent water columns. Although mixing processes may decay the amplitude of the zigzags, they are unlikely to greatly alter the spacing of the peaks in density space. Furthermore, we conclude that the points of the zigzags contain the least altered water, a conclusion tested with tracer data.

[80] Consideration of the CBL2002 data set indicates that the double-diffusive zigzag structures in both the Fram Strait Branch Water and the Barents Sea Branch Water can be used to fingerprint the boundary current and its interactions with neighboring waters. Over most of the CBLMR region, the core of the boundary current carries a ''point-and-bump'' θ-S structure, resulting from a combination of double diffusive and mechanical mixing processes. East of the Mendeleev Ridge, the outer edge of the boundary current has a large zigzag structure in θ-S space, reflecting interleaving of boundary current waters with older basin waters with rather different water mass properties. West of the Mendeleev Ridge, the zigzag structures are smaller in amplitude, implying interleaving between waters of more similar properties. Finally, ragged θ-S structures found over the Northwind Abyssal Plain imply older, ''relic'' waters.

[81] This approach allows us to define different regions with the CBLMR area. The newest waters in the boundary current are found to the west of the Mendeleev Ridge. In the Fram Strait Branch Water (FSBW), the temperature maximum is slightly colder than FSBW found elsewhere in the CBLMR region and this, combined with the small scale zigzags in this layer, indicate that boundary current is now supplying slightly colder water to this region than previously. This is consistent with the cooling of the FSBW which has been observed upstream in the Eurasian Basin. Changes are also evident in the Barents Sea Branch Water (BSBW) and deeper waters, although here the newest waters are also the coldest, freshest waters found in this layer in the CBLMR region.

[82] The data suggest that east of the Mendeleev Ridge at least a significant portion of the boundary current follows the topography to loop south around the Chukchi Abyssal Plain and then return northwards along the west side of the

Chukchi Rise. This flow is order 50 km wide, and found predominantly over isobaths from ca. 1500 m to 2500 m. This is similar to the boundary current properties found near the Lomonosov Ridge. Waters shallower show distinctly different properties, suggestive of shelf mixing. Waters deeper than this north of the Chukchi Rise show the interleaving of the boundary current waters with the adjacent, older basin waters.

[83] By 2002, it appears the warm core of the FSBW has progressed along the north side of the Chukchi Rise and reached the northeast of the Northwind Ridge. It is not possible from these data to ascertain how much of the boundary current is diverted northward or eastward into the deep basin from this region.

[84] The data do, however, show that the region of the Northwind Abyssal Plain is isolated, both topographically and in water properties, from the boundary current outside. Waters in this region are among the oldest found in this data set. Ventilation of this region appears to take place from the north, either along the eastern edge of the Chukchi Rise, or via topographic gaps to the north or east of the Abyssal Plain. These 2002 data do not show the warm FSBW core of the boundary current traversing through the Chukchi Gap (just north of the Chukchi Slope) and along the southern side of the Northwind Abyssal Plain.

[85] Dominant in these data is the strong topographical control of the flow patterns of the boundary current, even in regions of complex bathymetry such as the northern end of the Chukchi Rise and Northwind Ridge. This confirms the equivalent barotropic nature of the current. Although without velocity data we can do little more than speculate on flow velocities, is it evident that the time taken for the Atlantic waters to traverse this region is at least a few years, implying advective speeds of order 1–2 cm/s.

[86] There are, naturally, some caveats to this analysis. Throughout there is an assumption that the boundary current flow is reasonably steady, in an interannual sense. Further studies, including likely long-term measurements, theory and modeling will be necessary to show if this is a reasonable assumption.

[87] **Acknowledgments.** Our thanks go to the dedicated, professional and hardworking crew of the USCGC Polar Star and to the outstanding, tireless, highly motivated team of technicians and students who ensured the continuous high quality of this remarkable data set, even in trying circumstances. We are also extremely grateful to the Barrow Arctic Science Consortium and the North Slope Borough in Barrow for their logistical support of the cruise, and to the USCG especially Captain Dave Mackenzie, the Polar Star Marine Science team and the Science Liaison Officers LCDR April Brown and Dave Forcucci, for their focused dedication to getting the job done well. We thank Mike Steele for collegial discussions. The work was funded by NSF grants NSF-OPP-0117480, NSF-OPP-0117040, NSF-OPP-0117367, and NSF-ARC-0454843. Data are archived at NODC and via our website http://psc.apl.washington.edu/CBL.html.

References

Aagaard, K. (1989), A synthesis of the Arctic Ocean circulation, *Rapp. P.-V. Reun. Cons. Int. Explor. Mer.*, *188*, 11–22.

Aagaard, K., et al. (1996), U.S., Canadian researchers explore Arctic Ocean, *Eos Trans. AGU*, *77*, 209, 213.

Anderson, L. G., G. Bjork, O. Holby, E. P. Jones, G. Kattner, K. P. Koltermann, B. Liljeblab, R. Lindegren, B. Rudels, and J. Swift (1994), Water masses and circulation in the Eurasian basin: Results from the Oden 91 expedition, *J. Geophys. Res.*, *99*, 3273–3283.

Bormans, M., and C. Garrett (1989), A simple criterion for gyre formation by the surface outflow from a strait, with application to the Alboran Sea, *J. Geophys. Res.*, *94*, 12,637–12,644.

Carmack, E. C., R. W. Macdonald, R. G. Perkin, F. A. McLaughlin, and R. J. Pearson (1995), Evidence for warming of Atlantic water in the southern Canadian Basin of the Arctic Ocean: Results from the Larsen-93 expedition, *Geophys. Res. Lett.*, *22*, 1061–1064.

Carmack, E. C., K. Aagaard, J. H. Swift, R. W. MacDonald, F. A. McLaughlin, E. P. Jones, R. G. Perkin, J. N. Smith, K. M. Ellis, and L. R. Killius (1997), Changes in temperature and tracer distributions within the Arctic Ocean: Results from the 1994 Arctic Ocean Section, *Deep Sea Res., Part II*, *44*, 1487–1502.

Carmack, E. C., K. Aagaard, J. H. Swift, R. G. Perkin, F. McLaughlin, R. W. Macdonald, and E. P. Jones (1998), Thermohaline transitions, in *Physical Processes in Lakes and Oceans*, *Coastal Estuar. Stud.*, vol. 54, edited by J. Imberger, pp. 179–186, AGU, Washington, D. C.

Dickson, R. R., T. J. Osborn, J. W. Hurrell, J. Meincke, J. Blindheim, B. Adlandsvik, T. Vinje, G. Alekseev, and W. Maslowski (2000), The Arctic Ocean response to the North Atlantic Oscillation, *J. Clim.*, *13*, 2671–2696.

Falkner, K. K., M. Steele, R. A. Woodgate, J. H. Swift, K. Aagaard, and J. Morison (2005), Dissolved oxygen extrema in the Arctic Ocean halocline from the North Pole to the Lincoln Sea, *Deep Sea Res., Part I*, *52*, 1138–1154.

Frank, M., W. M. Smethie Jr., and R. Bayer (1998), Investigation of subsurface water flow along the continental margin of the Eurasian Basin using the transient tracers tritium, ^{3}He, and CFCs, *J. Geophys. Res.*, *103*, 30,773–30,792.

Gerdes, R., M. J. Karcher, F. Kauker, and U. Schauer (2003), Causes and development of repeated Arctic Ocean warming events, *Geophys. Res. Lett.*, *30*(19), 1980, doi:10.1029/2003GL018080.

Grotefendt, K., K. Logemann, D. Quadfasel, and S. Ronski (1998), Is the Arctic Ocean warming?, *J. Geophys. Res.*, *103*, 27,679–27,687.

Gunn, J. T., and R. D. Muench (2001), Observed changes in Arctic Ocean temperature structure over the past half decade, *Geophys. Res. Lett.*, *28*, 1035–1038.

Hunkins, K. (1966), Ekman drift currents in the Arctic Ocean, *Deep Sea Res.*, *13*, 607–620.

Jakobsson, M., C. Norman, J. Woodward, R. MacNab, and B. Coakley (2000), New grid of Arctic bathymetry aids scientists and map makers, *Eos Trans. AGU*, *81*, 89, 93, 96.

Jones, E. P. (2001), Circulation in the Arctic Ocean, *Polar Res.*, *20*, 139–146.

Jones, E. P., L. G. Anderson, and J. H. Swift (1998), Distribution of Atlantic and Pacific waters in the upper Arctic Ocean: Implications for circulation, *Geophys. Res. Lett.*, *25*, 765–768.

Karcher, M. J., R. Gerdes, F. Kauker, and C. Koberle (2003), Arctic warming: Evolution and spreading of the 1990s warm event in the Nordic seas and the Arctic Ocean, *J. Geophys. Res.*, *108*(C2), 3034, doi:10.1029/2001JC001265.

Killworth, P. D. (1992), An equivalent-barotropic mode in the Fine Resolution Antarctic Model, *J. Phys. Oceanogr.*, *22*, 1379–1387.

Klinger, B. A. (1993), Gyre formation at a corner by rotating barotropic coastal flows along a slope, *Dyn. Atmos. Oceans*, *19*, 27–63.

May, B. D., and D. E. Kelley (2001), Growth and steady state stages of thermohaline intrusions in the Arctic Ocean, *J. Geophys. Res.*, *106*, 16,783–16,794.

McDougall, T. J. (1985a), Double-diffusive interleaving. I. Linear stability analysis, *J. Phys. Oceanogr.*, *15*, 1532–1541.

McDougall, T. J. (1985b), Double-diffusive interleaving. II. Finite amplitude, steady state interleaving, *J. Phys. Oceanogr.*, *15*, 1542–1556.

McDougall, T. J. (1986), Oceanic intrusions - Some limitations of the Ruddick and Turner (1979) mechanism, *Deep Sea Res., Part A*, *33*, 1653–1664.

McLaughlin, F. A., E. C. Carmack, R. W. Macdonald, and J. K. B. Bishop (1996), Physical and geochemical properties across the Atlantic/Pacific water mass front in the southern Canadian basin, *J. Geophys. Res.*, *101*, 1183–1197.

McLaughlin, F., E. Carmack, R. Macdonald, A. J. Weaver, and J. Smith (2002), The Canada Basin, 1989–1995: Upstream events and far-field effects of the Barents Sea, *J. Geophys. Res.*, *107*(C7), 3082, doi:10.1029/2001JC000904.

McLaughlin, F. A., E. C. Carmack, R. W. Macdonald, H. Melling, J. H. Swift, P. A. Wheeler, B. F. Sherr, and E. B. Sherr (2004), The joint roles of Pacific and Atlantic-origin waters in the Canada Basin, 1997–1998, *Deep Sea Res., Part I*, *51*, 107–128.

McPhee, M. G., and J. D. Smith (1976), Measurements of the turbulent boundary layer under pack ice, *J. Phys. Oceanogr.*, *6*, 696–711.

Melling, H. (1998), Hydrographic changes in the Canada Basin of the Arctic Ocean, 1979–1996, *J. Geophys. Res.*, *103*, 7637–7645.

Morison, J., M. Steele, and R. Andersen (1998), Hydrography of the upper Arctic Ocean measured from the nuclear submarine USS Pargo, *Deep Sea Res., Part I*, *45*, 15–38.

Morison, J., K. Aagaard, and M. Steele (2000), Recent environmental changes in the Arctic: A review, *Arctic*, *53*, 359–371.

Nazarenko, L., T. Sou, M. Eby, and G. Holloway (1997), The Arctic ocean-ice system studied by contamination modelling, *Ann. Glaciol.*, *25*, 17–21.

Neshyba, S., V. T. Neal, and W. Denner (1971), Temperature and conductivity measurements under ice island T-3, *J. Geophys. Res.*, *76*, 8107–8120.

Padman, L., and T. M. Dillon (1987), Vertical heat fluxes through the Beaufort Sea thermohaline staircase, *J. Geophys. Res.*, *92*, 10,799–10,806.

Perkin, R. G., and E. L. Lewis (1984), Mixing in the West Spitsbergen Current, *J. Phys. Oceanogr.*, *14*, 1315–1325.

Pinkel, R. (2005), Near-inertial wave propagation in the western Arctic, *J. Phys. Oceanogr.*, *35*, 645–665.

Plueddemann, A. J., R. Krishfield, T. Takizawa, K. Hatakeyama, and S. Honjo (1998), Upper ocean velocities in the Beaufort Gyre, *Geophys. Res. Lett.*, *25*, 183–186.

Polyakov, I. V., G. V. Alekseev, L. A. Timokhov, U. S. Bhatt, R. L. Colony, H. L. Simmons, D. Walsh, J. E. Walsh, and V. F. Zakharov (2004), Variability of the intermediate Atlantic water of the Arctic Ocean over the last 100 years, *J. Clim.*, *17*, 4485–4497.

Polyakov, I. V., et al. (2005), One more step toward a warmer Arctic, *Geophys. Res. Lett.*, *32*, L17605, doi:10.1029/2005GL023740.

Proshutinsky, A., et al. (2005), Arctic Ocean Study: Synthesis of model results and observations, *Eos Trans. AGU*, *86*, 368, 371.

Quadfasel, D., A. Sy, D. Wells, A. Tunik, M. Tibayrenc, F. Kjellberg, and F. J. Ayala (1991), Warming in the Arctic, *Nature*, *350*, 385.

Quadfasel, D., A. Sy, and B. Rudels (1993), A ship of opportunity section to the North Pole: Upper ocean temperature observations, *Deep Sea Res., Part I*, *40*, 777–789.

Ruddick, B. R., and J. S. Turner (1979), The vertical length scale of double-diffusive intrusions, *Deep Sea Res., Part A*, *26*, 903–913.

Rudels, B. (1989), Mixing processes in the northern Barents Sea, *Rapp. P.-v. Réun. Cons. Int. Explor. Mer.*, *188*, 36–48.

Rudels, B., E. P. Jones, L. G. Anderson, and G. Kattner (1994), On the intermediate depth waters of the Arctic Ocean, in *The Polar Oceans and Their Role in Shaping the Global Environment*, edited by O. M. Johannessen et al., pp. 33–46, AGU, Washington, D. C.

Rudels, B., G. Björk, R. D. Muench, and U. Schauer (1999), Double-diffusive layering in the Eurasian Basin of the Arctic Ocean, *J. Mar. Sys.*, *21*, 3–27.

Schauer, U., R. D. Meunch, B. Rudels, and L. Timokhov (1997), Impact of eastern Arctic shelf waters on the Nansen Basin intermediate layers, *J. Geophys. Res.*, *102*, 3371–3382.

Schauer, U., B. Rudels, E. P. Jones, L. G. Anderson, R. D. Muench, G. Björk, J. H. Swift, V. Ivanov, and A. M. Larsson (2002), Confluence and redistribution of Atlantic water in the Nansen, Amundsen and Makarov basins, *Ann. Geophys.*, *20*, 257–273.

Shimada, K., F. McLaughlin, E. Carmack, A. Proshutinsky, S. Nishino, and M. Itoh (2004), Penetration of the 1990s warm temperature anomaly of Atlantic Water in the Canada Basin, *Geophys. Res. Lett.*, *31*, L20301, doi:10.1029/2004GL020860.

Smethie, W. M., Jr., P. Schlosser, G. Bonisch, and T. S. Hopkins (2000), Renewal and circulation of intermediate waters in the Canadian Basin observed on the SCICEX 96 cruise, *J. Geophys. Res.*, *105*, 1105–1121.

Smith, J. N., K. M. Ellis, and L. R. Kilius (1998), ^{129}I and ^{137}Cs tracer measurements in the Arctic Ocean, *Deep Sea Res., Part I*, *45*, 959–984.

Smith, J. N., K. M. Ellis, and T. Boyd (1999), Circulation features in the central Arctic Ocean revealed by nuclear fuel reprocessing tracers from Scientific Ice Expeditions 1995 and 1996, *J. Geophys. Res.*, *104*, 29,663–29,677.

Stern, M. E. (1967), Lateral mixing of water masses, *Deep Sea Res.*, *14*, 747–753.

Stern, M. E., and J. A. Whitehead (1990), Separation of a boundary jet in a rotating fluid, *J. Fluid Mech.*, *217*, 41–69.

Swift, J. H., E. P. Jones, K. Aagaard, E. C. Carmack, M. Hingston, R. W. MacDonald, F. A. McLaughlin, and R. G. Perkin (1997), Waters of the Makarov and Canada basins, *Deep Sea Res., Part II*, *44*, 1503–1529.

Swift, J. H., K. Aagaard, L. Timokhov, and E. G. Nikiforov (2005), Long-term variability of Arctic Ocean waters: Evidence from a reanalysis of the EWG data set, *J. Geophys. Res.*, *110*, C03012, doi:10.1029/2004JC002312.

Toole, J. M., and D. T. Georgi (1981), On the dynamics and effects of double-diffusively driven intrusions, *Prog. Oceanogr.*, *10*, 123–145.

Turner, J. S. (1965), Coupled turbulent transports of salt and heat across sharp density interface, *Int. J. Heat Mass Transfer*, *8*, 759–767.

Walsh, D., and E. Carmack (2002), A note on evanescent behavior of Arctic thermohaline intrusions, *J. Mar. Res.*, *60*, 281–310.

Walsh, D., and E. Carmack (2003), The nested structure of Arctic thermohaline intrusions, *Ocean Modell.*, *5*, 267–289.

Walsh, D., and B. Ruddick (1995), Double-diffusive interleaving: The influence of nonconstant diffusivities, *J. Phys. Oceanogr.*, *25*, 348–358.

Walsh, D., and B. Ruddick (1998), Nonlinear equilibration of thermohaline intrusions, *J. Phys. Oceanogr.*, *28*, 1043–1070.

Woodgate, R. A., K. Aagaard, R. D. Muench, J. Gunn, G. Bjork, B. Rudels, A. T. Roach, and U. Schauer (2001), The Arctic Ocean Boundary Current along the Eurasian slope and the adjacent Lomonosov Ridge: Water mass properties, transports and transformations from moored instruments, *Deep Sea Res., Part I*, *48*, 1757–1792.

Woodgate, R. A., K. Aagaard, J. H. Swift, W. M. Smethie, and K. K. Falkner (2003), Chukchi Borderland Cruise CBL2002 Arctic West - Phase II (AWS-02-II), 51 pp., Univ. of Wash., Seattle. (Available at http://psc.apl.washington.edu/CBL.html)

Woodgate, R. A., K. Aagaard, J. H. Swift, K. K. Falkner, and W. M. Smethie (2005), Pacific ventilation of the Arctic Ocean's lower halocline by upwelling and diapycnal mixing over the continental margin, *Geophys. Res. Lett.*, *32*, L18609, doi:10.1029/2005GL023999.

Yang, J. (2006), The Arctic and Subarctic-Ocean flux of potential vorticity and the Arctic Ocean circulation, *J. Phys. Oceanogr.*, in press.

Zhang, J., D. A. Rothrock, and M. Steele (1998), Warming of the Arctic Ocean by a strengthened Atlantic inflow: Model results, *Geophys. Res. Lett.*, *25*, 1745–1748.

K. Aagaard and R. A. Woodgate, Polar Science Center, Applied Physics Laboratory, University of Washington, 1013 NE 40th Street, Seattle, WA 98105, USA. (woodgate@apl.washington.edu)

K. K. Falkner, College of Oceanic and Atmospheric Sciences, Oregon State University, Corvallis, OR 97331-5503, USA.

W. M. Smethie Jr., Lamont-Doherty Earth Observatory of Columbia University, Palisades, NY 10964, USA.

J. H. Swift, Scripps Institution of Oceanography, University of California, San Diego, CA 92093-0214, USA.